Co-funded by the European Union

HyUSPRe

Hydrogen **U**nderground **S**torage in **P**orous **Re**servoirs

New experimental data on reactions between H_2 and well cement and effects on fluid flow and mechanical properties of well cement

Prepared by: Anisa Noor Corina
Vincent Soustelle
Jan ter Heege

TNO Applied Geosciences, Princetonlaan 6, Utrecht, The Netherlands

Please cite this report as: Corina, A.N., Soustelle, V. & Ter Heege, J.H. 2023: Report with new experimental data on reactions between H_2 and well cement and effects on fluid flow and mechanical properties of well cement, H2020 HyUSPRe project report. 37 pp.

The authors would like to thank Rama Kotni (TNO), Wouter van de Steeg (TNO), and Al Moghadam (TNO) for the support on the experimental works and critical feedback.

This report represents HyUSPRe project deliverable number D5.2.
A supplementary Excel file [doi 10.5281/zenodo.7808431; HyUSPRe_D5.2_Supplement_Test protocol] contains all relevant experimental data as part of the open access policy of the HyUSPRe project.

The HyUSPRe consortium

Funded by

Acknowledgement

This project has received funding from the Fuel Cells and Hydrogen 2 Joint Undertaking (now Clean Hydrogen Partnership) under grant agreement No 101006632. This Joint Undertaking receives support from the European Union's Horizon 2020 research and innovation programme, Hydrogen Europe and Hydrogen Europe Research.

Disclaimer

Executive summary

In this study, new experimental data is presented of the effects of H_2 exposure and cyclic loading on mechanical properties of oilwell (class G) cement, relevant for underground hydrogen storage operations. Changes in mechanical properties (Young's modulus, Poisson's ratio and ultimate strength) have been analyzed using unconfined compressive strength (UCS) tests and confined cyclic loading tests on class G cement samples that were unreacted (cured for 3 days at 80°C) and exposed to lime-saturated brine and N_2 or H_2 for 1 and 2 months. Changes in cement mineralogy were analyzed by XRD analysis of the unreacted and exposed samples.

The mechanical properties of elastic modulus and Poisson's ratio are within the expected range of an oilwell cement. Differences in Young's modulus, Poisson's ratio and ultimate strength are limited between unreacted, N_2-exposed and H_2-exposed samples, when comparing UCS tests or confined cyclic loading tests. Repeated UCS tests seem to indicate that the variation in Young's modulus and ultimate strength increases after N_2 and H_2 exposure, but this observation needs to be confirmed in additional tests. During cyclic axial loading of confined cement samples, irreversible (plastic) deformation (compaction) occurs that affect static Young's modulus. Also, effects of exceeding yield and failure strength on Young's modulus are observed. Dynamic Young's moduli and Poisson's ratios derived from acoustic velocity measurements during confined cyclic tests show limited variation, in particular if static and dynamic Young's modulus are compared. The mineralogical changes as identified using XRD analysis suggest minor changes between unexposed and H_2- and N_2-exposed samples, although XRD patterns indicate some minerals that could not be identified.

The main conclusion is that effects of H_2 exposure and cyclic loading on mechanical properties and mineralogical changes of class G cement is limited compared to unreacted or N_2 exposed samples for the investigated conditions. There is no indication that changes in mechanical properties of cement are such that cement integrity of wells used for underground hydrogen storage will be significantly affected. It should be emphasized that this conclusion is based on experiments on one type of cement (class G) and a limited set of conditions. In particular, additional tests to assess the reproducibility of current results and tests on samples that were exposed longer to H_2 and N_2 are of interest. Detailed effects of changing properties for the durability and integrity of wells can be derived by performing a parameter sensitivity analysis with well integrity modelling for the range in mechanical properties measured in this study.

About HyUSPRe

Hydrogen **U**nderground **S**torage in **P**orous **Re**servoirs

The HyUSPRe project researches the feasibility and potential of implementing large-scale underground geological storage for renewable hydrogen in Europe. This includes the identification of suitable porous reservoirs for hydrogen storage, and technical and economic assessments of the feasibility of implementing large-scale storage in these reservoirs to support the European energy transition to net zero emissions by 2050. The project will address specific technical issues and risks regarding storage in porous reservoirs and conduct an economic analysis to facilitate the decision-making process regarding the development of a portfolio of potential field pilots. A techno-economic assessment, accompanied by environmental, social, and regulatory perspectives on implementation will allow for the development of a roadmap for widespread hydrogen storage by 2050, indicating the role of large-scale hydrogen storage in achieving a zero-emissions energy system in the EU by 2050.

This project has two specific objectives. Objective 1 concerns the assessment of the technical feasibility, associated risks, and the potential of large-scale underground hydrogen storage in porous reservoirs for Europe. HyUSPRe will establish the important geochemical, microbiological, flow, and transport processes in porous reservoirs in the presence of hydrogen via a combination of laboratory-scale experiments and integrated modelling; and establish more accurate cost estimates to identify the potential business case for hydrogen storage in porous reservoirs. Suitable storage sites will be identified, and their hydrogen storage potential will be assessed. Objective 2 concerns the development of a roadmap for the deployment of geological hydrogen storage up to 2050. The proximity of storage sites to large renewable energy infrastructure and the amount of renewable energy that can be buffered versus time varying demands will be evaluated. This will form a basis for developing future scenario roadmaps and preparing for demonstrations.

Document information, revision history, approval status

Document information

Title:	D5.2 [New experimental data on reactions between H2 and well cement and effects on fluid flow and mechanical properties of well cement]
Lead beneficiary:	TNO
Contributing beneficiaries:	TNO
Due date:	M17 [28/02/2023]
Dissemination level:	Public
Published where:	HyUSPRe website
Recommended citation:	Corina, A.N., Soustelle, V. & Ter Heege, J.H. 2023: Report with new experimental data on reactions between H2 and well cement and effects on fluid flow and mechanical properties of well cement, H2020 HyUSPRe project report. 37 pp.

Revision history

Version	Name	Delivery date	Summary of changes
V01	A. Corina	2023.02.06	Draft report delivered to WP lead
V02	J. ter Heege	2023.02.10	Reviewed & modified draft to WP leads & industry partners
V03	J. ter Heege	2023.02.27	Finalize report, incorporated comments industry partners
V04	H. Cremer	2023.02.27	Final report for upload to SygMa
V05	H. Cremer	2023.04.07	DOI for data supplement added on cover page

Approval status

Role	Name	Delivery date
Deliverable responsible:	A. Corina	2023.02.06
Task leader:	A. Corina	2023.02.06
WP leader:	J. ter Heege	2023.02.10
HyUSPRe lead scientist	R. Groenenberg	2023.02.27
HyUSPRe consortium manager:	H. Cremer	2023.02.27

Table of Content

1 Introduction

1.1 Deliverable context

Within the HyUSPRe project the feasibility of large-scale storage of renewable hydrogen in porous reservoirs is investigated, including assessment of technical issues and risks. Research on technical issues and risks focusses on geochemical (WP2), microbiological (WP3), flow and transport (WP4), and geomechanical (WP5) processes that control the response of the subsurface porous reservoir storage system to cyclic injection and withdrawal of a hydrogen-containing gas stream. A combination of laboratory-scale experiments and integrated modelling will be performed to assess this response. In WP5, focus is on geomechanical processes, i.e. effects of cyclic injection and withdrawal of a hydrogen-containing gas stream that affect the durability and integrity of well systems and reservoir and seals.

The current report (D5.2) describes experiments that have been performed within Task 5.2 of the HyUSPRe project. This task focusses on the effects of hydrogen and cyclic loading on well systems. Well systems can be leakage pathways for hydrogen if not properly constructed, or if operations critically affect zonal isolation. New experimental data are presented that analyse the effects of hydrogen and cyclic loading on the mechanical properties of well cement at (downhole) pressure, temperature and stress conditions relevant to porous reservoirs. The data extends existing experimental data on the effect of H_2 on well cement as reviewed in deliverable D5.1 (Corina et al. 2022).

1.2 Scientific background

Underground hydrogen storage (UHS) in porous subsurface reservoirs requires cyclic operations of injection and withdrawal of a hydrogen-containing gas stream. These operations can have three main effects on well systems (1) cyclic variation in pore pressure, temperature and associated changes of stress on the well system causing the casing, cement sheath, and formation to contract and expand alternately, (2) long term exposure of hydrogen-rich gas streams to well materials that may change the mechanical properties of well materials due to reactions with hydrogen, and (3) interactions with rock and well materials at the reservoir level such as microbiological or chemical reactions may lead to by-products that enhance degradation or erosion of well materials (in particular, enhanced corrosion of steel well components by formation of H_2S). The interaction between cyclic changes in stresses on well systems and chemical reactions between well materials and hydrogen may particularly affect the integrity of well barriers such as wellhead components, injection/withdrawal (‘production’) tubing and well cement (see Corina et al. 2022 and references therein). During cyclic injection and withdrawal of a hydrogen-containing gas stream, the wellhead and injection/withdrawal (‘production’) tubing are exposed to hydrogen and/or hydrogen by-products. Therefore, many studies focus on interaction of hydrogen (by-products) with different steels. Also, steel-hydrogen interaction has been studied extensively within the framework of hydrogen transport through pipelines or storage in steel tanks. Well cement provides mechanical support for the well system within reservoir and overburden as well as protection of steel casings against reactive or corrosive formation fluids or gases. Accordingly, both mechanical and chemical interaction may affect cement integrity as annular cement may be exposed to chemical attacks by hydrogen (by-products) and physical loads from thermal or pressure changes in the wellbore and reservoir. Cement integrity is important to maintain zonal isolation along wells and prevent migration pathways along fractured cement or rock-cement-casing interfaces. Issues with zonal isolation caused by loss of cement integrity are notoriously difficult to mitigate. Depending on the severity of cement intergity issues, functionality of a well for injection or withdrawal of a hydrogen-containing gas stream may be jeopardized which will

dramatically affect efficiency and lifetime of hydrogen storage projects. Based on vast experience with long term seasonal storage of natural gas, these issues are often considered of limited importance if relatively low concentrations (< ~10%) of hydrogen are co-mixed with natural gas streams in existing underground gas storage projects with demonstrated durability, integrity and efficiency of operations (i.e. it is assumed that wells will maintain functionality as demonstrated during cyclic injection and withdrawal of natural gas). However, the combined effects of cyclic loading and hydrogen reactions on the mechanical properties of well cement are not yet studied in detail. In particular, data for larger concentrations of hydrogen in the gas stream are lacking.

1.3 Effects of hydrogen on properties of well cement

Different types of cements are used for cementation of casings in well systems (usually class A-H cement according to the classification outlined in API Spec 10A, 2010), depending on specific subsurface pressure and temperature conditions and/or resistance against chemical interaction with (for example H_2S, see also Smith 2003). Below, we review the main studies that investigate potential effects of hydrogen on the properties of well cement. Most studies focus on changes in chemistry, mineralogy, and fluid flow properties such as porosity and permeability. Despite its importance for cement integrity and durability, analysis of effects on the mechanical properties of well cement is largely lacking.

The hydrogen reactivity to the class G cement was previously simulated using the geochemical thermodynamics calculation by Jacquemet et al. (2020). Major cement minerals Calcium silicate hydrates (CSH) and $Ca(OH)_2$ (portlandite) are non-redox-sensitive minerals, and hence their volume fraction is unchanged after reaction with hydrogen. Meanwhile, minor cement minerals of ettringite and hematite are redox-sensitive and encounter full reductive dissolution with H_2. The produced sulphides from ettringite reduction and the ferrous iron from hematite reduction combine to precipitate mackinawite (FeS). Moreover, the remaining ferric iron in hematite combines with the ferrous iron to precipitate ferric-ferrous iron oxide magnetite (Fe_3O_4). The precipitation of FeS and Fe_3O_4 is estimated to reduce the cement matrix volume after reaching full thermodynamic equilibrium.

Existing experimental studies investigating the influence of H_2 on cement properties are summarised in Table 1. The project Underground Sun Storage (2020) reported that cement gas permeability increases after being exposed to H_2 for 2 to 14 months, but the increase is insignificant (typically increased by a factor 1.2-1.7). Accordingly, the final permeability is in the same order as the initial permeability. The final gas permeability of these samples is also in the same order as those exposed to CH_4 and blank gas of N_2, and the increase is attributed to leaching of cement and reaction with CO_2 in the mixing water. The phase identification on the H_2-exposed sample shows that the vaterite ($CaCO_3$ polymorph) content increases after exposure, which contributes to a reduction in cement permeability and likely limits increase of permeability during exposure.

Shi et al. (2020) showed that gas permeability of H_2-exposed cement samples can increase by 62.5% despite a drop in porosity by 0.4%. The accompanying XRD analysis showed that the Portlandite and calcite content increases after the sample is exposed, which is similar to the observation by Underground Sun Storage (2020). A similar trend of increasing permeability and porosity reduction after H_2 exposure was reported by Boersheim et al. (2019), although observed changes in permeability and porosity are more substantial than in other studies. The final permeability and porosity of samples exposed to H_2 and N_2 are roughly similar. After exposure, the pH of the in-situ fluid increased from pH 5 to 11 and the concentration of calcium increased, both suggesting cement leaching during exposure.

Table 1. Summary of experimental works evaluating cement properties in a hydrogen system.

Study by	Cement mixture	Hydrogen mixture & exposure method	Exposure condition	Studied parameters
Underground Sun Storage (2020)	N/A	25% H_2 and 75% CH_4 The wet gas (i.e. gas passing through an activated water-saturated carbon) is circulated through cement samples.	40 °C and 70 bars Period: < 14 months	Gas permeability, XRD analysis
Boersheim et al. (2019)	Neat cement Class G (44% BWOC)	100% H_2 Cement samples are submerged in a brine bath while pressurised with gas.	100 C and 50 bars. Period: 4 weeks	Gas permeability, porosity
Shi et al. (2020)	N/A	13% H_2 and 87% NG (96.4% methane) Cement samples are conditioned in an autoclave under dry conditions (i.e. not submerged in brine) while pressurised with gas.	80 C and 262 bars. Period: 3 months	Gas permeability, porosity, XRD analysis
(Corina & ter Heege, 2021)	Neat cement Class G (38% BWOC)	99.9% H_2 Cement samples are submerged in a brine bath (8% NaCl) while pressurised with gas	80-110 C and 200 bars. Period: 2 weeks	Uniaxial compressive strength, Young's Modulus, Poisson's ratio

The influence of hydrogen exposure on cement's mechanical properties was reported by Corina and ter Heege (2021) in preliminary work preceeding the HyUSPRe project and experiments of Task 5.2. The properties were measured in the unconfined compressive strength (UCS) test, and the results are indicated in Table 2. The highest compressive strength is observed in the N_2-exposed sample, followed by the H_2-exposed and unexposed samples, consecutively. The elastic modulus of these samples varies between 8.7 and 11.3 GPa. However, reproducibility tests were not performed which hampered definite conclusions on effects of hydrogen exposure on the mechanical properties of well cement.

Table 2. Summary of mechanical properties of neat cement (38% BWOC) in different exposure conditions (Corina and ter Heege, 2021).

Sample	Exposure	UCS (MPa)	Young's modulus (E) [GPa]	Poisson's ratio (ν) [-]
2.1	No exposure	39.2	8.7*)	0.087*)
2.2	N_2 exposure	56.3	10.8	0.121
2.3	H_2 exposure	47.2	11.3	0.127

1.4 Current study of effects of H_2 on cement mechanical properties

The findings of the three studies summarised above show that the influence of H_2 on the hydraulic properties of cement is insignificant at studied conditions (pressure, temperature, exposure time). There is limited information on the influence of hydrogen on the mechanical properties of well cement. Additionally, the exposure procedures were also observed to influence the cement properties, which may influence the effects during hydrogen exposure. For example, prolonged cement exposure under dry conditions (or conditions of low relative humidity) could induce microcracking due to the shrinkage following pore water evaporation. The influence of micro cracks on the cement mechanical properties will be more pronounced in smaller samples. Moreover, prolonged exposure to low-pH fluid, including tap water, can cause the cement to leach due to the dissolution of Portlandite and CSH, which will alter fluid flow and mechanical properties. Impurities in the liquid, such as CO_2, can also react with cement minerals, which will change the cement properties as well. Therefore, it is essential to perform the exposure test in a controlled environment that minimizes leaching and reactions unrelated to hydrogen exposure. Also, reproducibility tests and benchmarking of H_2 exposure

against samples exposed to inert gases (such as N_2) are important to be sure that observed changes are not due to cement sample variability or exposure to fluids or gases in general.

The goal of the current experiments with task 5.2 is to identify the changes in the mechanical properties of well cements exposed to H_2. The experimental program consists of a reaction test (autoclave exposure test), mechanical unconfined compressive strength (UCS) and cyclic loading test (uniaxial and triaxial deformation tests), and cement phase identification (XRD analysis). In the reaction test, cement samples of neat Class-G are exposed to H_2 gas at high pressure and temperature to simulate the condition of UHS in porous reservoirs at a depth of ~2000 m. For comparison, several samples are exposed to inert gas (N_2) at the same pressure and temperature conditions, while another sample set is kept unexposed. Following the reaction test, the UCS test is performed on all samples to measure the ultimate strength and elastic properties (Young's modulus and Poisson's ratio). In addition to the UCS test, a cyclic test is performed to simulate the pressure changes associated with injection and production phases in UHS. In the cyclic test, a series of stress loading-unloading cycles are applied on unexposed and exposed samples while monitoring the change in elastic properties. In addition to the mechanical tests, the mineralogical phases of unexposed and exposed cement samples are identified through XRD.

2 Materials and methodology

2.1 Cement specimens

As suffient sample material of cement from actual wellbores or field sites to perform a systematic series was not available, synthetic cement samples were prepared following the standard procedure for cement testing outlined in API RP 10 B. The cement samples are prepared from neat cement slurry, composed of Class-G, 44% BWOC (by weight of cement) of water, and without any additives. The slurry is mixed (15 s at ~4000 rpm followed by 35 s at ~12000 rpm in a cement mixer) and poured into cylindrical PTFE moulds with an inner diameter of ~25 mm. The slurry is placed in stages and mixed slowly with paddles to eliminate entrapped air bubbles. The moulds were sealed and then placed inside a water bath that has been preconditioned at a temperature of 80°C. After 3 days of curing, the samples were cooled down, removed from the mould, and preserved in saturated lime water (pH 12.4) at room temperature to prevent leaching. Some of the cement samples are preserved to be used as a reference. Three different batches of samples were prepared (indicated by A, B, C in sample labels) as the number of samples that can be prepared in a single batch is limited.

The use of synthetic cement samples has the advantage of consistent, standardized sample preparation that limits heterogeneity within samples and variability between samples. However, it likely differs from properties of cement in sheaths surrounding casings after well cementation operations. Also, the state and properties of well cement changes over time due to long term curing, mechanical loading or chemical degradation due to interaction with formation or injected fluids such as CO_2 (see, for example, Watson and Bachu 2009; Szabó-Krausz et al. 2020; Yousuf et al. 2021). To some extent these long term effects can be mimicked in laboratory experiments by changing curing conditions prior to exposure and mechanical tests. In particular, elevated temperatures accelerate reactions during curing of cement. In this study, curing conditions (3 days at 80°C and ambient pressure) were chosen as previous studies showed limited changes in compressive strength after curing class-G cement for 3 days at 80°C (see, for example, Zhang et al. 2014). The temperatures are also within the range of temperatures expected at 2.0-2.5 km depth, albeit pressure history during curing is different.

2.2 Reaction tests

The cement samples for reaction testing were separated into two groups that were conditioned in an autoclave and exposed to working fluids of H_2 and N_2, respectively. The cement sample was contained inside a PP tube and submerged in a brine mixture. A small hole was created on the cap of the tube to allow the gas to be in contact with the brine Figure 1. The brine mixture (Table 3) has a density of around 1.16 g/cm^3. The brine mixture is saturated with lime ($Ca(OH)_2$) to prevent cement leaching and has a pH of around 12.3. The working gas, N_2 or H_2 (99%), was pumped into the autoclaves until the pressure of 200 bars is reached. The temperature of the autoclaves was set at 80 ^oC. These conditions simulate the downhole condition of a production casing cement at a depth of approx. 2000 m. It also represents the P90 of reservoir conditions of UGS wells collected in WP1 of the HyUSPRe project.

Figure 1. (Left) PP tubes filled with cement sample and placed inside the autoclave (right).

Table 3. Brine composition for reaction test.

Composition	Dissolved salt (g/l)
NaCl	162.6
KCl	2.9
$CaCl_2$	40.4
$MgCl_2$	5.3

After 1 month of exposure, some samples were removed from the autoclaves, and the remainder was removed after a total of 2 months of exposure. When removing samples from the autoclave, the autoclaves were depressurised and cooled down at a very low rate to not damage the samples. The test matrix of mechanical testing and mineralogical analysis of each group is in Table 4.

Table 4. The test matrix of mechanical testing and mineralogical analysis for different exposure conditions.

Sample condition	# Total samples	# Samples for planned test			
		XRD	UCS	Cyclic test	**Total**
H_2 / 1 month	5	-	2	-	2
H_2 / 2 month	5	1	2	1	4
N_2 / 1 month	6	-	2	-	2
N_2 / 2 month	5	1	2	1	4
Unreacted cement	8	1	2	1	4

2.3 Mechanical tests

The mechanical tests are performed using a GDS triaxial load frame (Figure 2). Prior to testing, the samples were cut to produce a cylindrical sample with a length (L) of approx. 50 mm. The surface of the cores was polished to generate parallel, flat end surfaces. Two types of mechanical tests were conducted, i.e. unconfined compressive strength (UCS) tests and confined tests with cyclic changes in differential stress on the samples (cyclic tests).

The following sensors were installed to measurements sample displacement, axial load (force), confining pressure and sample pressure (Figure 2):

- External force required to deform sample as measured by an external load cell mounted to top of the load frame (250 kN pancake type load cell with accuracy of 0.1% of full range output, Figure 2a). Internal force required to deform sample as measured by an internal load cell mounted to the upper (balanced) ram inside the triaxial cell (250 kN submersible load cell with accuracy of 0.1% of full range output).
- Position triaxial cell relative to the upper (balanced) ram as measured by a linear displacement transducer mounted on the upper ram (linear strain type transducer with accuracy <0.075%). Samples were deformed by moving the triaxial assembly against the fixed crosshead at constant displacement rate of loading ram which compresses the sample between the bottom piston and upper (balanced) ram
- Local axial and radial displacement sensors (LVDT's) were mounted on the sample. For the UCS tests, axial displacement is determined by two axial LVDT's that measure relative displacement of two rings mounted on the top and bottom piston, and radial displacement is determined using an LVDT that measures extension of a ring placed around the central part of the sample with a metal spring (Figure 2b). For the cyclic tests, axial displacement is measured by two axial LVDT's mounted on the top piston, and radial displacement is determined using two LVDT's that measure extension of two half rings of aluminium placed around the central part of the sample with a mounting piece and two metal springs (Figure 2c).
- For the UCS tests, samples were loaded in uniaxially (i.e., the apparatus were operated without a confining medium). Samples were open to atmosphere during testing (i.e., no attempt was taken to control sample humidity or temperature) and conducted at room temperatures. For the cyclic tests, samples were jacketed using polyolefin shrinking tube (2:1 shrinking ratio, 18 N/mm2 tensile strength), silicone oil was used as confining medium, confining pressure was applied using an external high pressure syringe pumps to control pressure/volume of the oil, and sample pressure was applied using a second external high pressure syringe pumps to control pressure/volume of water at the sample ends.
- The axial force (F_a), confining pressure (P_c) and sample pressure (P_p) measured by the internal load cell and pressure pumps are used to calculate axial stress $\sigma_1 = F_a/A + P_c$ (with A the sample area), differential stress $\Delta\sigma = \sigma_1 - \sigma_2$ (with $\sigma_2 = \sigma_3 = P_c$), and effective stress $\sigma_x' = \sigma_x - P_p$ (x = 1, 2, 3 for maximum, intermediate and minimum principal stress, respectively).
- In the cyclic tests, acoustic velocities are measured using transducers embedded into the top cap and the pedestal holding the top and bottom pistons, respectively (Figure 2c) which comprise 3 piezo-electric plates. The first is for generating/receiving P-waves signals and the two others, oriented a 90° to each other, are used for generating/receiving S-waves signals. The transducers from the pedestal and the top cap are used for generating and receiving waves signals, respectively. The waves were pulsed generated at frequency of 1 MHz and the data were recorded and processed.

In the UCS test, an unconfined sample is placed in the pressure cell and axially loaded in the load frame at a constant strain rate of $1x10^{-5}$ s^{-1} until the sample reaches its ultimate strength before failure. Besides measuring the ultimate strength, the stress and strain response during axial loading are used to calculate Young's modulus and Poisson's ratio. For each exposure condition, two samples were tested.

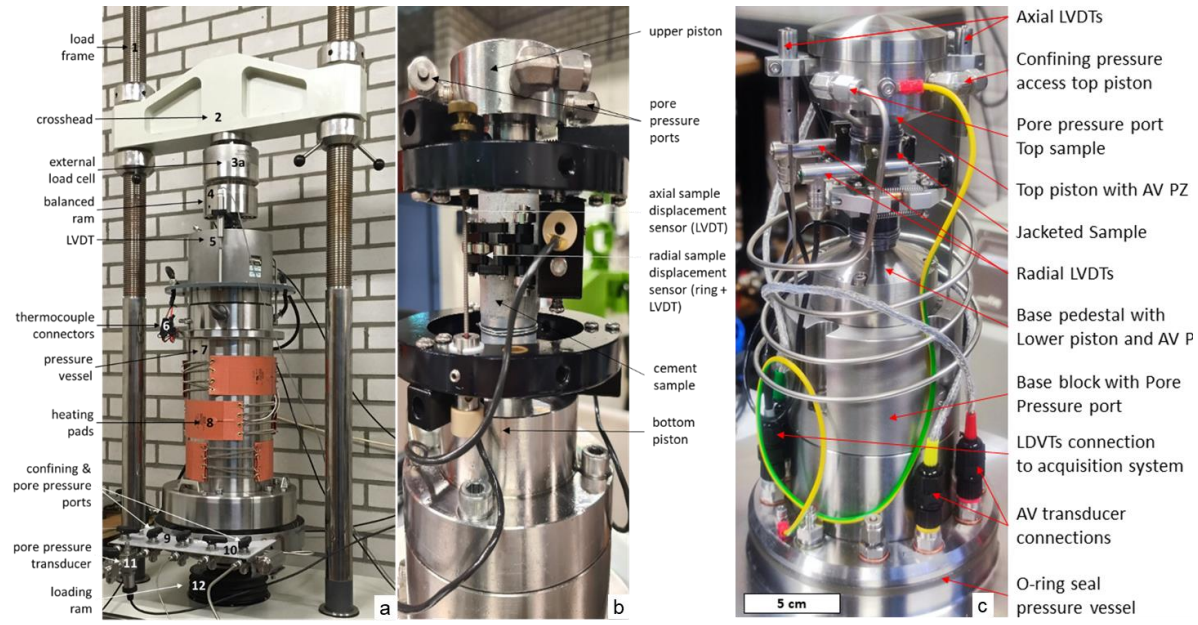

Figure 2. (a) Triaxial load frame and pressure cell. (b) Sample setup for UCS tests. (c) Sample setup for cyclic tests with acoustic velocity sensors (AV). Both sample setup are placed inside the triaxial pressure cell (comparable to) the cell shown in (a).

The cyclic test simulates the performance of the cement sheath between the production casing and the caprock during the pressure change due to the cycle of gas injection and production. To enable testing at representative stress conditions, the minimum and maximum bottom hole pressure (BHP) of a UHS are first determined with the following steps and assumptions:

- The change (Δ) in maximum and minimum reservoir pressure, which are based on the collected UGS data from WP1, that meets P90 is selected.
- The minimum reservoir pressure for UHS is assumed 50-60 bars lower than for UGS, based on density differences between methane and hydrogen and data and models from WP1.
- The minimum and maximum BHP are estimated with a 10% margin to the minimum and maximum reservoir pressure, respectively.

The stresses of the cement sheath are then calculated using the in-house modeling tool (CReST) based on the selected BHP range (1 scenario). The subsurface condition, e.g. caprock properties, for the model input is based on the available information of Dutch subsurface condition at a depth of approx. 2000 m, combined with general assumptions. The outcome is adopted for the protocol of the cyclic test.

For the cyclic test, the cement sample is confined (σ_3) at 8 MPa. A pore pressure (P_p) of 1 MPa is applied and kept constant during the test (i.e. drained test). At the initial stage, the sample is axially loaded to reach a differential stress ($\Delta\sigma = \sigma_1' - \sigma_3'$) of 15 MPa. This approximates the initial stress state of cement at downhole conditions. Afterwards, the axial stress is cyclically changed to $\Delta\sigma$ of 4 (unloading) and 15 MPa (loading) for 12 times. At every cycle and during the loading, acoustic measurement is run to generate the shear and compressional wave velocity through the sample. The readings are used to calculate the dynamic Young's modulus and Poisson's ratio. After completion of the unloading-loading cycles, the axial load is increased step-wise to $\Delta\sigma$ of 20, 30, and 40 MPa. At each step, an acoustic measurement

is run. Finally, the sample is loaded until reaches the ultimate strength and unloaded to $\Delta\sigma$ approx. 2 MPa.

Strain rate during loading and unloading in the cyclic test are constant (approx. 1 x 10^{-5} s^{-1}). An example of the time series of a cyclic test is shown in Figure 3. The cyclic test was run on one sample from each of the 3 groups of unreacted, H_2/2 months, and N_2/2 months samples (Table 4).

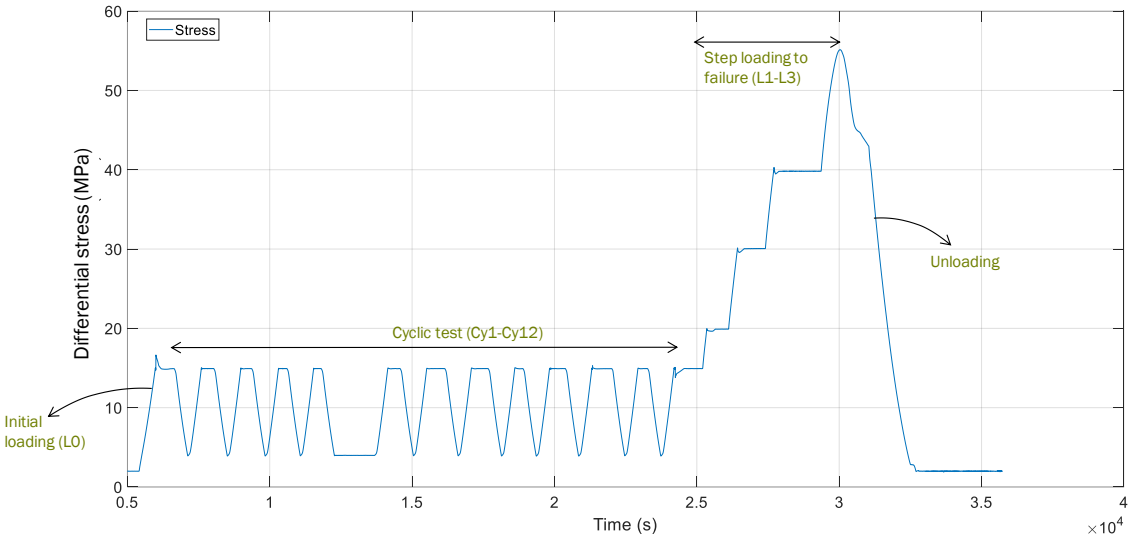

Figure 3. The time series of a cyclic test of sample A15 (H_2/2 months).

2.4 Mineralogical identification

The phase identification of the samples is performed by qualitative XRD analysis. The analysis was performed on one sample from unreacted and 2-month exposed samples, as shown in Table 4. For the exposed samples, the analysis was performed twice using the parts from the top and bottom of the sample. Diffraction patterns were recorded using a Bruker D8 Advance X-ray diffractometer in Bragg-Brentano geometry. Cu-Kα X-rays were generated at 40 kV and 40 mA. To limit exposure of the samples to possible moisture and the atmosphere a sample stage was used which includes a controlled atmosphere and humidity chamber. Before mounting the sample the chamber was flushed with dry nitrogen. During the analysis, a steady and low flow of dry nitrogen continued through the chamber. No attempts were made to perform a quantitative XRD analysis using an internal standards.

3 Results

3.1 Visual observations of exposed samples

After the reaction test was concluded, the samples were visually observed to identify changes. In general, the brine level in the PP tubes of some samples was observed to slightly drop after exposure (Figure 4a). The drop in the brine level was presumed due to the water uptake due to continuing cement hydration and change in moisture content due to the high temperature. White precipitation was observed at the bottom of the brine and occasionally at the sample surface because of the tapered shape of the sample. The white precipitation is presumed to be calcium hydroxide $Ca(OH)_2$. The limewater-saturated brine was initially prepared at room temperature, and as the temperature in the autoclave increased, the solubility of $Ca(OH)_2$ reduces and the fluid pH slightly drops. The latter was confirmed by pH measurement on the residual brine that shows values ranging between 11.5-12.0. The visual observations of samples exposed to H_2 and N_2 are similar, and there was no difference between those exposed for 1 month and 2 months period (Figure 4b).

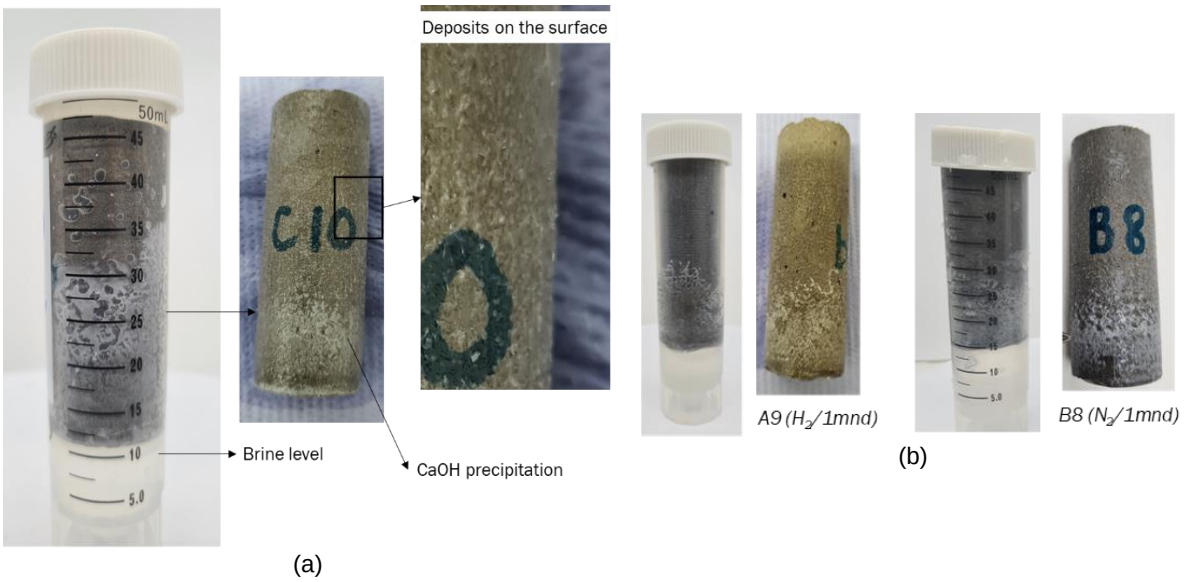

Figure 4. (a) The visual observation of sample C10 after being submerged in brine and exposed to H2 after 2 months, and (b) observation of samples A9 and B8.

3.2 UCS tests

The summary of the results from the UCS test is shown in Table 5. The UCS values of each sample grouped based on the exposure condition are presented in Figure 5. It was observed that the averaged UCS of the H_2-exposed samples (32.2 MPa) is smaller than the unreacted samples (37.2 MPa), and smaller than the N_2-exposed samples (39.2 MPa) after 1 month of exposure. A similar trend is also observed for the 2-month exposed samples; the averaged UCS of the H_2-exposed samples is the smallest at 32.8 MPa, whereas the average for N2-exposed samples is 38.9 MPa. However, it should be noted that the UCS value from the same repetition tends to vary. The biggest variation is observed in samples that are exposed for 2 months.

Table 5. The summary of the sample properties: density, UCS, Young's modulus, and Poisson's ratio. Labels A, B, C in the sample names indicate different batches of prepared samples.

Sample	Group	Density (gr/cm^3)	UCS (MPa)	E (GPa)	v
B2	Unreacted	1.87	37.0	7.4	0.14
C2	Unreacted	1.92	37.4	6.4	0.21
B8	N_2 / 1 month	1.96	45.5	8.2	0.22
B5	N_2 / 1 month	1.92	32.8	6.6	0.26
A17	N_2 / 2 month	1.95	27.7	2.5	0.46
C9	N_2 / 2 month	1.95	50.2	10.2	0.36
C18	H_2 / 1 month	1.95	28.2	2.6	0.29
A9	H_2 / 1 month	1.93	36.3	6.5	0.40
C10	H_2 / 2 month	1.93	45.2	9.6	0.28
A4	H_2 / 2 month	1.98	20.5	1.7	0.33

The averaged Young's modulus and Poisson's ratio of the samples are presented in Figure 6. The averaged modulus of the N_2-exposed samples for 1 and 2 months is 7.4 GPa and 6.4 GPa, respectively. The values are relatively close to the unreacted sample with 6.9 MPa, although large variation is observed for 2 months N_2 exposure. The averaged Young's modulus of the H_2-exposed samples after 1- and 2- month exposure is 4.6 and 5.7 GPa, respectively. They are smaller than the N_2-exposed and unreacted samples. Similar to the observation of UCS values, the elastic moduli vary considerably between repeated tests. The averaged Poisson's ratio of both N_2- and H_2-exposed samples is ranging between 0.24-0.4, and they are higher than those of unexposed samples (0.17).

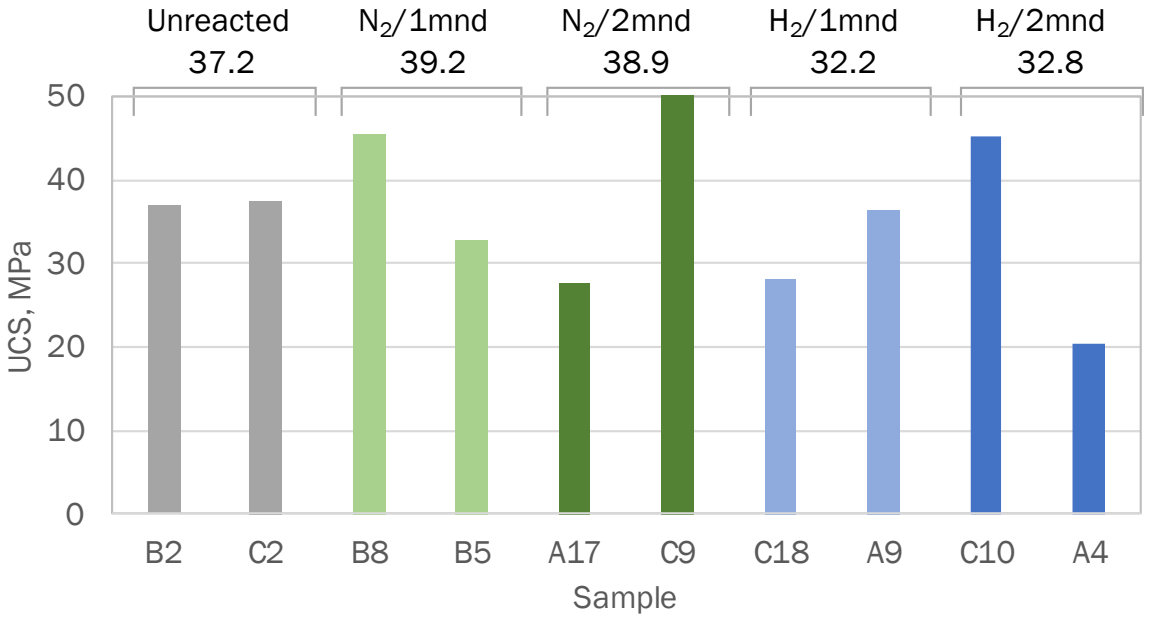

Figure 5. UCS values of the samples grouped based on the exposure condition and duration. The values above the bars show the averaged UCS (in MPa). Labels A, B, C in the sample names indicate different batches of prepared samples.

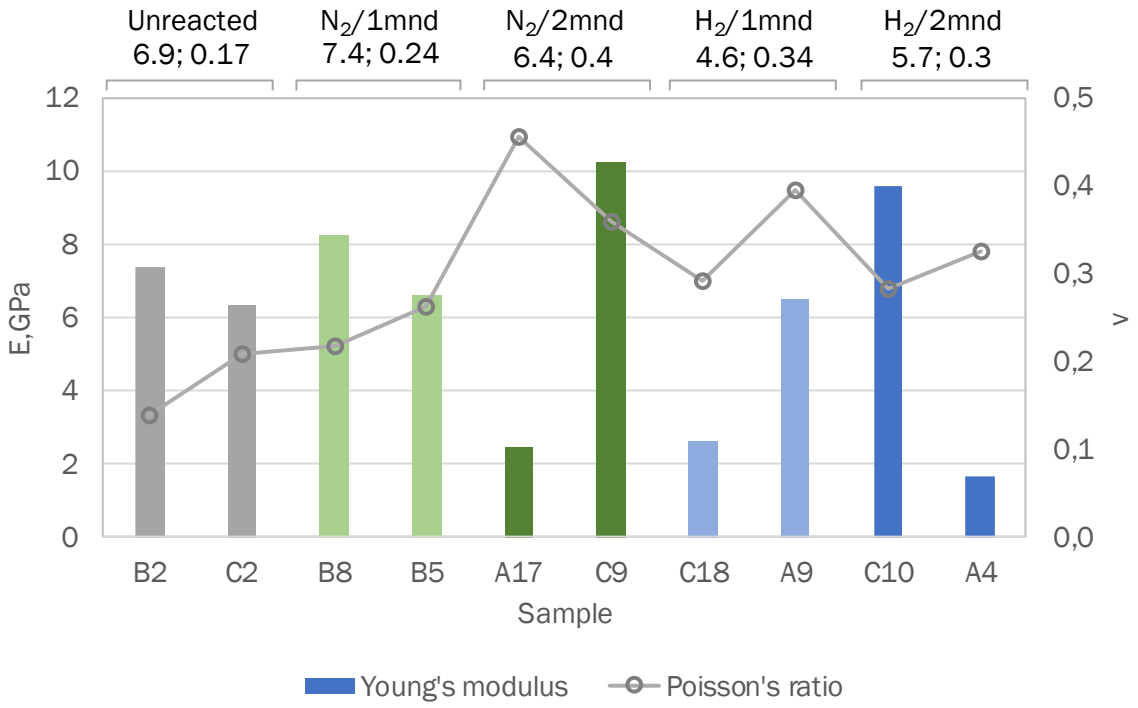

Figure 6. Young's modulus and Poisson's ratio of the samples grouped based on the exposure condition and duration. The values above the bars show the averaged Young's modulus (in GPa) and Poisson's ratio, respectively. Labels A, B, C in the sample names indicate different batches of prepared samples.

3.3 Cyclic tests

The results of the static and dynamic Young's modulus and dynamic Poisson's ratio from the cyclic test are summarised in Figure 7. The loading stage includes the initial loading (L0), the loading during the stress cycles (Cy-1 until Cy-12), and the step-wise stress loading (L-1 until L-3). Whereas, the unloading stage includes the unloading during the stress cycles (Cy-1 until Cy-12) and the unloading after the sample reaches the ultimate strength (cf. Figure 3). The static Young's modulus is calculated for both loading- and unloading stages, whereas the dynamic moduli and Poisson's ratio are based on acoustic velocity measurements during the loading stages.

General observations from all test samples show that the static elastic modulus increases sharply from the initial loading (L0) to the first cycle (Cy-1). The static modulus of samples C6 (unreacted) and A1 (N_2/2 months) increases by approx. 2 GPa, which is twice higher than the increase in sample A15 (H_2/2 months). After the first cycle, the static modulus increases gradually until cycle 12 (Cy-12). In addition, the static moduli measured during unloading and loading in all cycles have similar values. In the first step loading of L-1 ($\Delta\sigma$ = 20 MPa), the static modulus increases sharply and then decreases in the loading of L-2 ($\Delta\sigma$ = 30 MPa) and L-3 ($\Delta\sigma$ = 40 MPa). Sample C6 and A1 have similar values of static modulus; both have an initial static modulus of approx. 6 GPa and the moduli increase to 8.5-9.0 GPa as the cycles progress. Moreover, the static modulus of both samples during the final unloading is comparable at approx. 6.5 GPa. Sample A15, on the other hand, has a higher static modulus. The static modulus is 8.6 GPa during the initial loading and ultimately increases to 9.8 GPa after 12 cycles. The static modulus during the final unloading reduces sharply to 6.9 GPa.

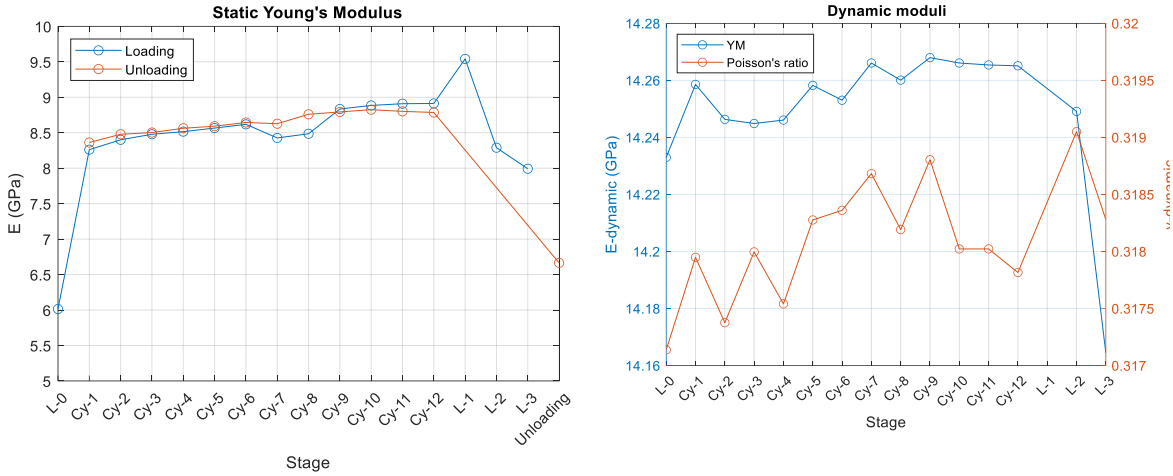

(a) Sample C6 – unreacted

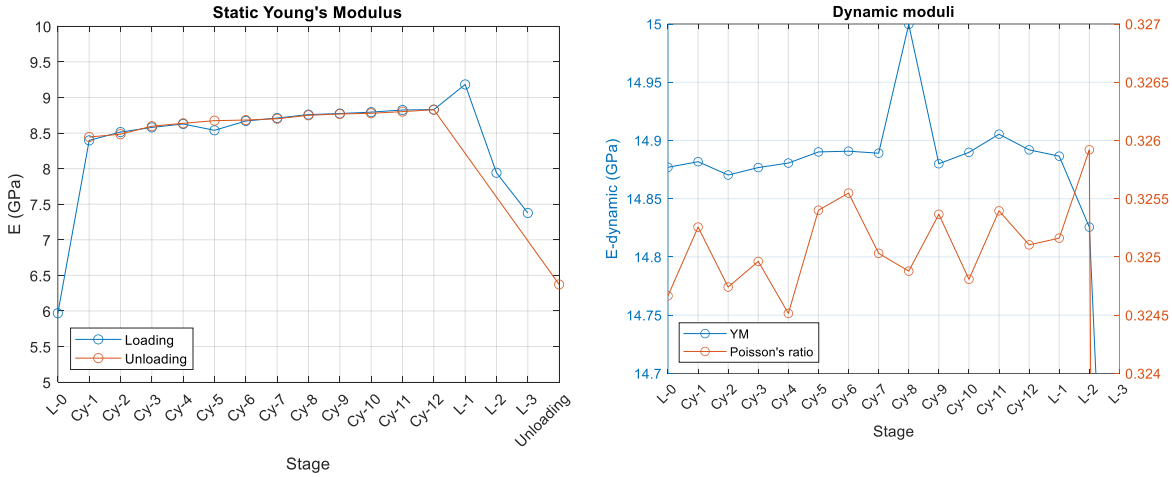

(b) Sample A1 – N_2/2 month

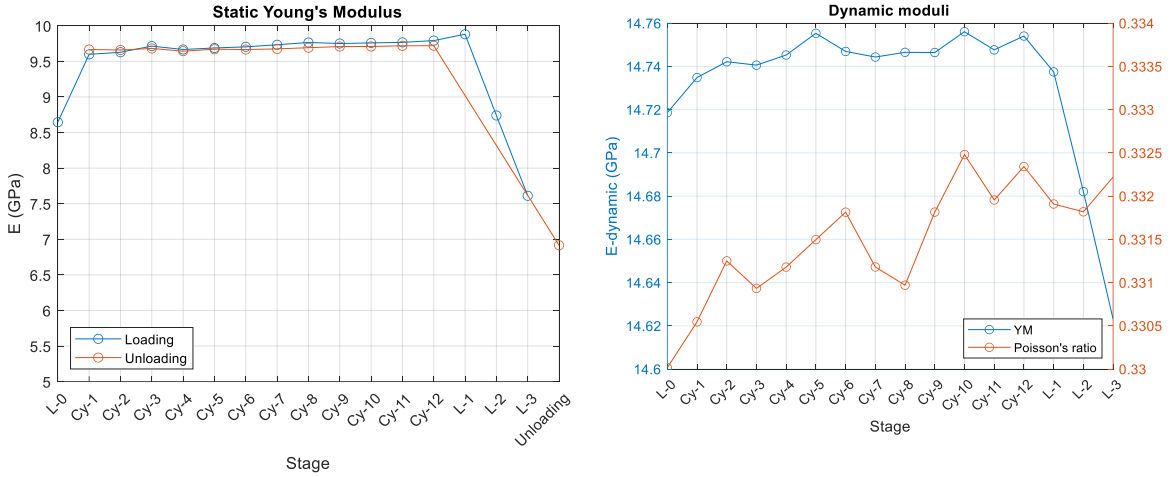

(c) Sample A15 – H_2/2 month

Figure 7. Static Young's modulus (left) during the unloading and loading stage in the series of the cyclic test and dynamic Young's modulus and Poisson's ratio from the acoustic velocity measurement during the loading stage for samples C6 (a), A1 (b), and A15 (c). The notation of the stage reflects those indicated in Figure 3. The unloading stage is measured after sample failure.

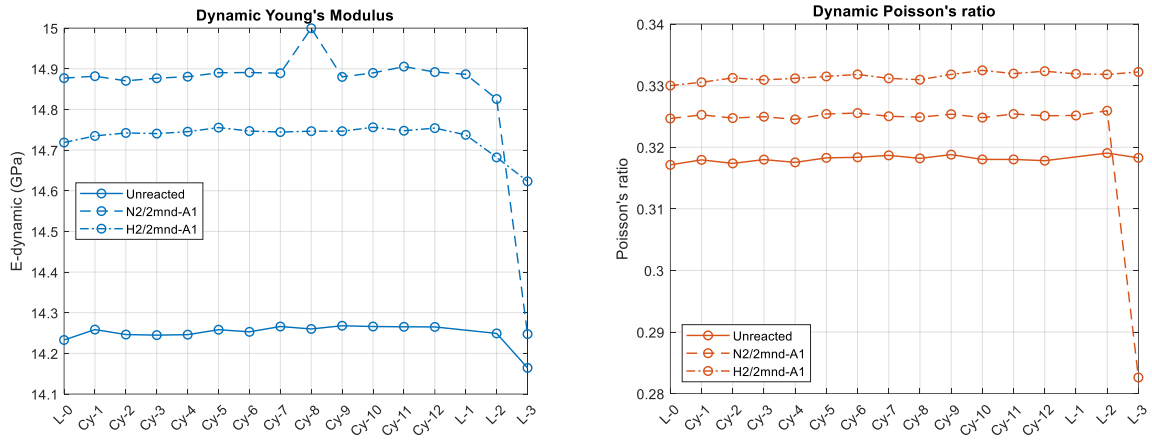

Figure 8. Dynamic Young's modulus and Poisson's ratio of all samples C6 (unreacted), A1 (H_2/2 month), and A15 (N_2/2 month).

The initial dynamic Young's modulus (YM) of all samples is consistent at 14-15 GPa, and the difference between each sample is maximum 0.6 GPa (Figure 8). YM slightly increases as the cycles progress. This trend is similar to the static modulus, although the increase of dynamic modulus is less steady and much smaller, only at the order of 10^{-2} GPa (within measurement error). The dynamic Poisson's ratio also shows a trend of increasing with cycles at the order of 10^{-3} (within measurement error). As the increase is within measurement error, the increase could be due to minor changes in the sample-piston-jacket assembly (e.g., alignment or jacket shrinkage/expansion) and/or due to changes in the mechanical properties of the sample.

The ultimate strength measured at the end of the cyclic test is presented in Table 6**Error! Reference source not found.**. Sample A15 has a slightly lower ultimate strength at 53.6 MPa than sample C6 and A1 with 55.4 and 55.1 MPa, respectively. The difference in the ultimate strength is insignificant, considering sample variability and measurement error.

Table 6. The density and ultimate strength of samples tested in a confining stress of 8 MPa and pore pressure of 1 MPa.

Sample	Group	Density (gr/cm^3)	Ultimate strength (MPa)
C6	Unreacted	1.92	55.4
A1	N_2 / 2 month	1.97	55.1
A15	H_2 / 2 month	1.95	53.6

3.4 Mineralogical analysis

The XRD analysis of the unreacted, N_2/2 months-, and H_2/2 months- samples is shown in Figure 9, Figure 10, Figure 11, respectively. Figure 8 shows that the major phases of the unexposed cement sample are unhydrated phases of alite (C_3S), ferrite phase or brownmillerite (C_4AF), and hydrated phases of Portlandite ($Ca(OH)_2$), katoite (C_3ASH_4), and hibschite. These phases are also present in both H_2- and N_2-exposed samples. Halite (NaCl) was present in the reacted samples, and is due to brine infiltration. Brucite ($Mg(OH)_2$) was only observed in the bottom part of the H_2-exposed sample.

Several unidentified peaks are present in the samples. In unreacted samples, peaks at approx. 14.5º, 14.9º, 16.3º, and 17.3º are identified, but the intensity of these peaks is significantly reduced in the reacted samples. Other unidentified peaks that are identical in all samples are

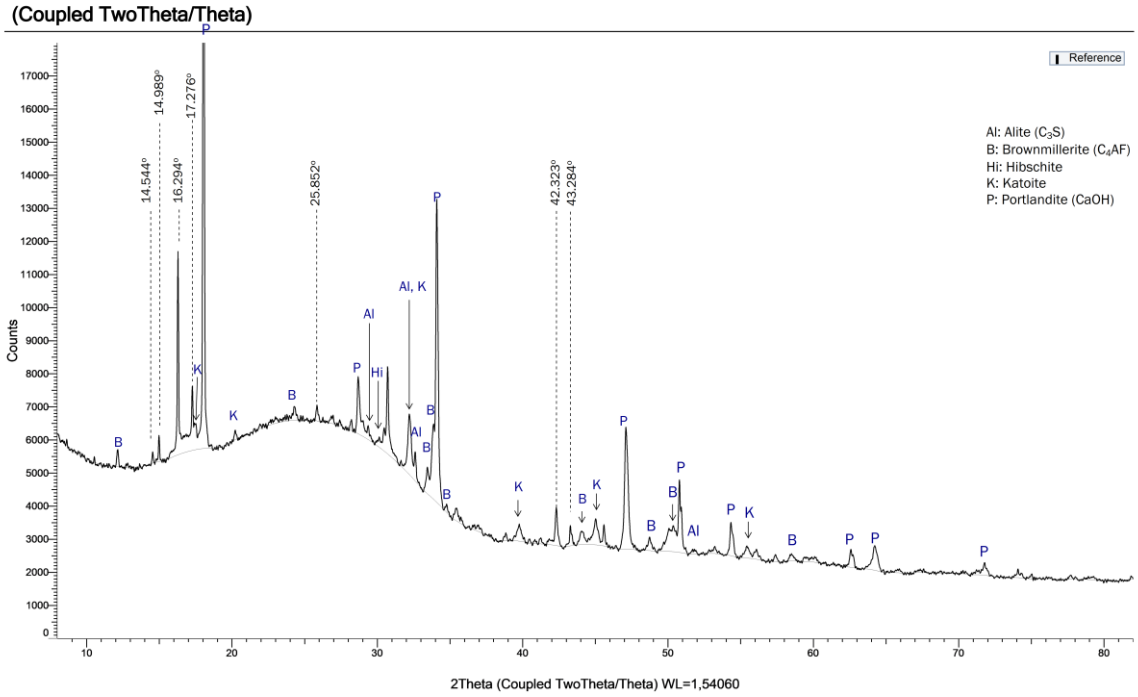

Figure 9. X-ray powder diffraction patterns of the major phase of unexposed class G cement samples. Unidentified peaks are identified with its 2θ values.

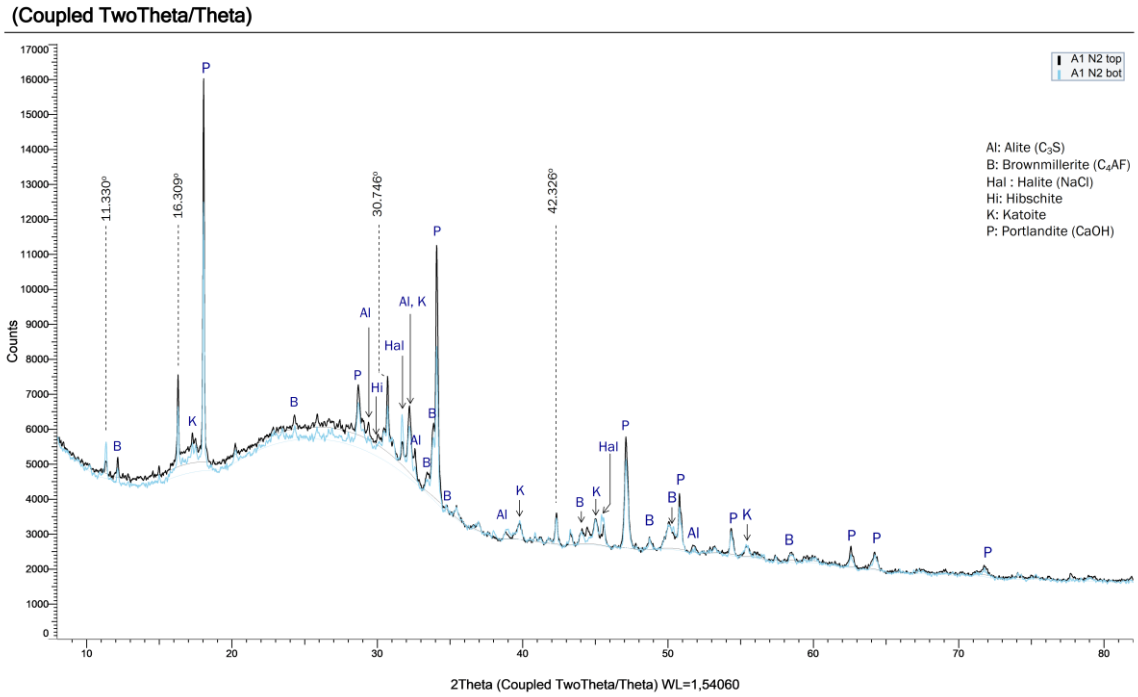

Figure 10. X-ray powder diffraction patterns of the major phase of the N_2-exposed class G cement sample taken from the top and bottom of the core. Unidentified peaks are identified with its 2θ values.

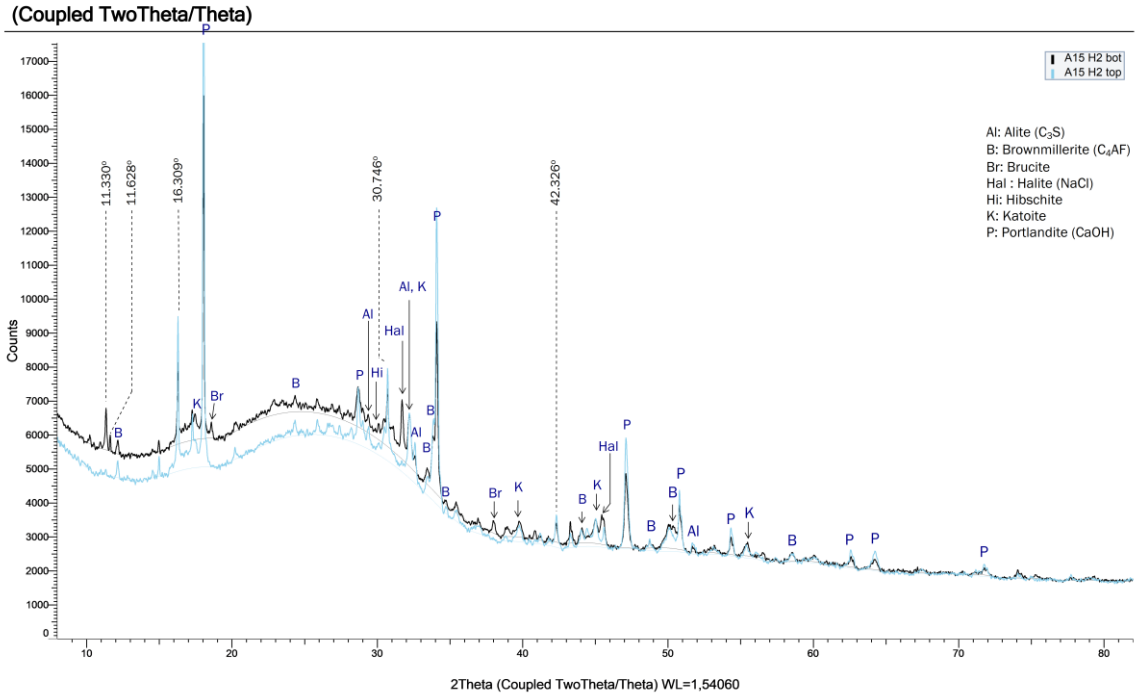

Figure 11. X-ray powder diffraction patterns of the major phase of the H_2-exposed class G cement sample taken from the top and bottom of the core. Unidentified peaks are identified with its 2θ values.

located at 25.8º, 42º, and 43º. Further calibration of XRD diffraction patterns from benchmark samples of pure mineral phases present in cement, or comparison with other studies of cement mineralogy using XRD analysis could help interpretation of the changes in diffraction patterns. As the current study focussed on analyzing changes in mechanical properties of cement, such extensive calibration is beyond the scope of this study.

4 Discussion

4.1 Effects of H_2 exposure and cyclic loading on the mechanical properties of well cement

From the UCS test, it was observed that the average ultimate strength of H_2-exposed samples is smaller by 5-6 MPa than the N_2-exposed and unreacted samples. However, the difference in strength can be due to sample variability as repeated UCS tests on H_2-exposed samples shows values of 20-45 MPa. Repeated UCS tests on N_2-exposed samples show ultimate strength values of 28-50 MPa, while variation in unreacted samples is limited (37.0-37.4 MPa). Given the variation in UCS for N_2- and H_2-exposed samples, consistent trends in UCS with H_2 exposure are not apparent. Limited variability of unreacted samples should be confirmed in additional tests. If limited variation in ultimate strength of unreacted samples is confirmed in additional tests, the effect of N_2 and H_2 exposure is an increased variability in ultimate strength. Differences between N_2 and H_2 exposure are not clear due to the variability in ultimate strength after exposure. Effects could be due to an interplay of different processes, such as (1) variation in sample porosity and permeability, (2) ongoing cement curing at elevated pressure and temperature, (3) sample compaction or dilatation, (4) infiltration of brine, N_2 or H_2, and (5) reactions with H_2. The relative importance of these processes are unclear. These observations demonstrate the importance of reproducibility tests in analyzing the effect of exposure on mechanical properties of cement samples.

Sample variability can be due to local variations in porosity (or trapped air) and permeability, which is expected to be reduced when the sample is confined. The confinement provides support to the sample by preventing spontaneous and unstable brittle failure and early collapse and crack propagation due to the sample heterogeneity. Considering that well cement will be under confinement at reservoir conditions, ultimate strength measured with the sample subjected to a confining pressure will be more relevant for in situ conditions. The ultimate strength of cement samples under a confining pressure of 8 MPa was measured in the cyclic tests. Results show that the ultimate strength of sample A15 (H_2/2 months) is only slightly smaller by approx. 2 MPa than that of samples C6 (unreacted) and A1 (N_2/2 months), which both are around 55 MPa. The difference between the H_2-exposed samples and unreacted- and N_2-exposed samples seem less significant with the sample was tested under confinement. It should be noted that reproducibility tests were not performed so variability between multiple unreacted, and N_2- or H_2-exposed samples could not be determined.

Static Young's modulus from UCS tests show similar changes in variability of values between unreacted (6.4-7.4 GPa) and N_2-exposed (2.5-10.2 GPa) or H_2-exposed (2.6-9.6 GPa) samples as for ultimate strength, i.e. variation in values increases if samples are exposed to brine with N_2 or H_2. The static Young's modulus measured during the initial loading (L0) of the cyclic tests for the unreacted and N_2/2 months-exposed samples (6.0-6.9 GPa) and for the H_2/2 months-exposed samples (5.9 GPa) is within the range of values from the UCS tests. The dynamic Young's modulus measured during the initial loading (L0) in the cyclic test are consistent for all samples (14.2-14.9 GPa). The dynamic Young's modulus from acoustic velocity measurements is larger than the static modulus (factor of 1.7-2.5). Other studies also reported that dynamic modulus values from acoustic measurements are either equal to or higher than the static values. Reddy et al. (2007) showed that the dynamic moduli are approx. 1.6 times than the static moduli.

Results from all cyclic confined tests show that the static elastic modulus increases sharply in the first stress cycle and more gradually with further cycles. The increase in elastic modulus is likely mainly due to the sample compaction and porosity reduction, which eventually resulting

a stiffer material. Existing literature also reported a similar observation of increasing elastic modulus with stress cycles (Kuanhai et al., 2020; Zhou et al., 2019). Results from all samples also show that the static modulus increases by ~0.5 GPa when the axial load is increased to $\Delta\sigma$ = 20 MPa but reduces sharply to 6.4-7.0 GPa at $\Delta\sigma$ = 30 MPa. This drop in Young's modulus after increasing axial load in the final cycles is likely caused by development of internal fractures after the sample has reached the yield strength at $\Delta\sigma$ = 30 MPa. The static modulus during unloading is similar to that during loading at each stage of the stress cycle. This indicates that the hysteresis during the unloading and loading is minimal, consistent with cumulative compaction and associated increase in Young's modulus during subsequent cycles prior to reaching yield strength. Values for dynamic Young's modulus and Poisson's ratio are also increasing with initial loading (L0) subsequent cycles (Cy-1 to Cy-12), notably with more variation including drops in values in some cycles. The variation in Young's modulus values is much smaller than for static Young's modulus, and within measurement error. Interestingly, the increase in Young's modulus during initial loading is less apparent for the dynamic Young's moduli. Also, the increase in static Young's modulus during loading L1 is not observed for the dynamic Young's modulus where values decrease during L1-L3. Apparently, measured acoustic velocities and calculated dynamic elastic moduli are not as sensitive to changes in the cement samples as static elastic moduli. This observation may help interpretation in studies that analyze changes in elastic properties of well cement using acoustic velocity measurements.

4.2 Deviation from elastic sample deformation

When deriving Young's modulus and Poisson's ratio from UCS or cyclic tests, it is assumed that cement samples deform according to linear elasticity theory. Changes in elastic moduli during initial loading and load cycles indicate that plastic deformation (compaction and/or fracturing) occurred. As many models treat well cement as a linear elastic material, it is important to analyze the importance of plastic deformation during cement deformation. Compaction (volume reduction) and plastic strain can be analyzed from the cyclic tests to indicate the importance of plasticity in sample deformation.

The volumetric deformation (compaction) of the samples during the loading and unloading phase in the cyclic test is shown in Figure 12. Positive values indicate volume reduction of the sample. As radial strain measurements in the cyclic tests showed large variations, the volumetric deformation is calculated using measured axial strain and radial strain calculated from the axial strain and dynamic Poisson's ratio. The volumetric deformation during unloading is taken to be representative of irreversible (plastic) volumetric deformation in the sample. The cumulative increase in volumetric deformation, both during loading and unloading, during subsequent stress cycles indicates that the samples are gradually compacted. Large compaction is observed when the axial load was increased in loading phases L1-L3. The cumulative compaction up to loading phase L1 is accompanied by an increasing Young's Modulus (i.e. increasing stiffness of cement). Ongoing compaction during L2-L3 where the decrease in static Young's modulus is indicating that the yield strength is exceeded is likely an artefact from calculating radial strain using dynamic Poisson's ratio. Unless the sample failed by pore collapse, dilatation is expected when the yield strength of the sample is exceeded. As mentioned in section 4.1, dynamic elastic moduli calculated from acoustic velocity measurement are not reflecting sample failure contrary to static Young's modulus.

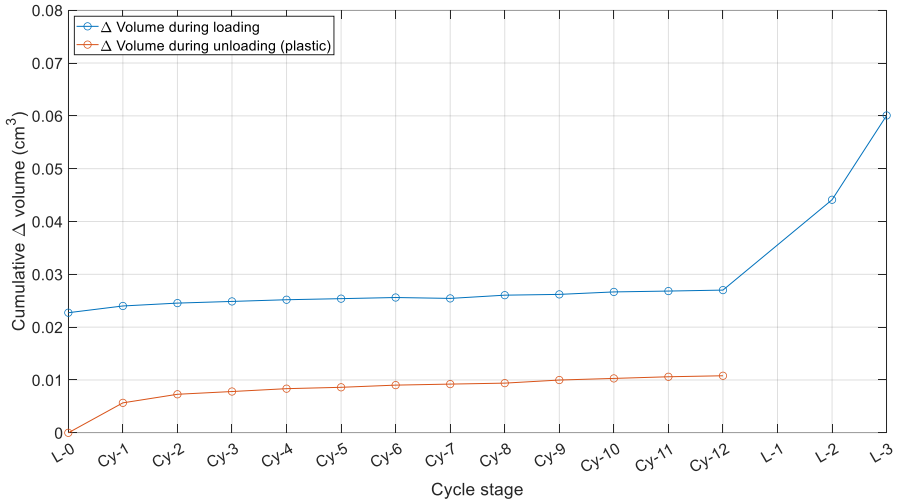

(a) Sample C6 – unreacted

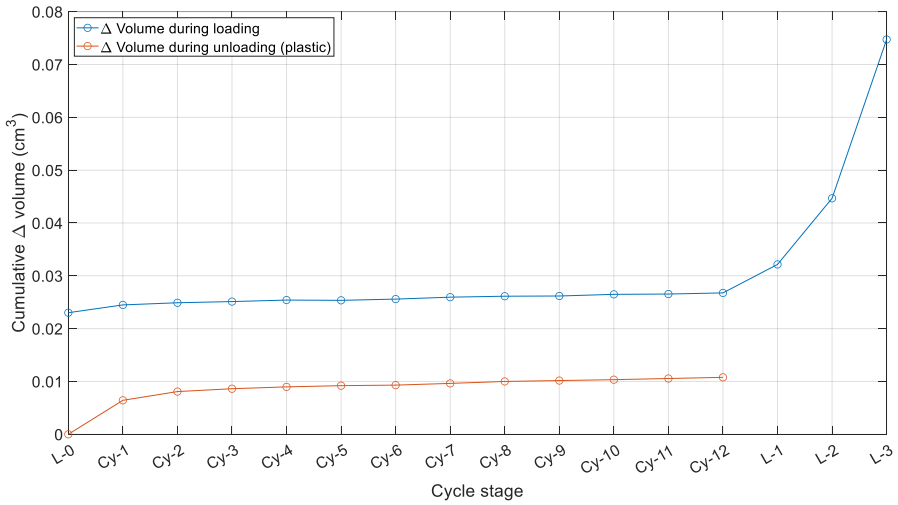

(b) Sample A1 – N_2/2 month

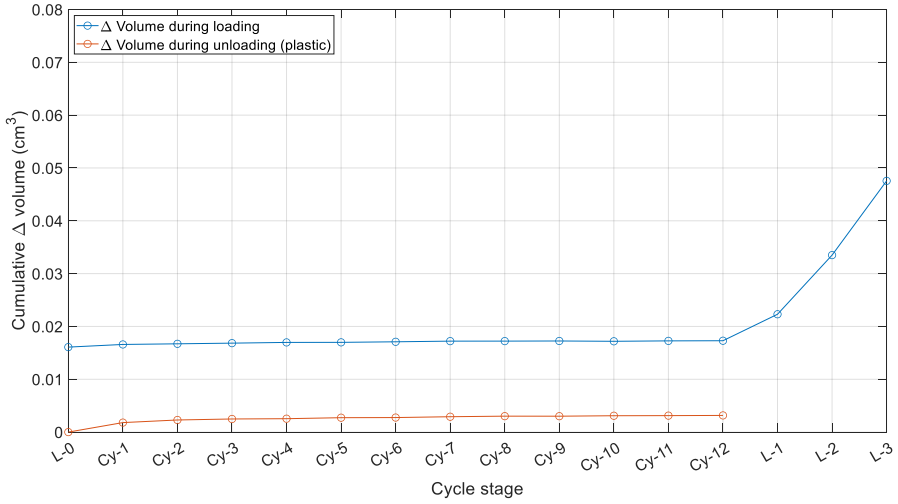

(c) Sample A15 – H_2/2 month

Figure 12. Volumetric deformation from the cyclic test of samples (a) C6, (b) A1, and (c) A15.

The amount of cumulative irreversible axial deformation (plastic axial strain) after each cycle of unloading-loading is also calculated and plotted in Figure 13. In all samples, it was observed that the biggest irreversible deformation occurs after the unloading from the initial loading. The irreversible deformation reduces with increasing cyclic stage. After 12 cycles, the plastic strain of samples C6 and A1 is around 0.12 %, whereas it is much smaller for sample A15 with 0.035% (Figure 14). The smaller plastic strain in sample A15 (H_2/2 month exposure) is associated with a higher static Young's modulus than the unreacted and N_2/2 month exposed samples.

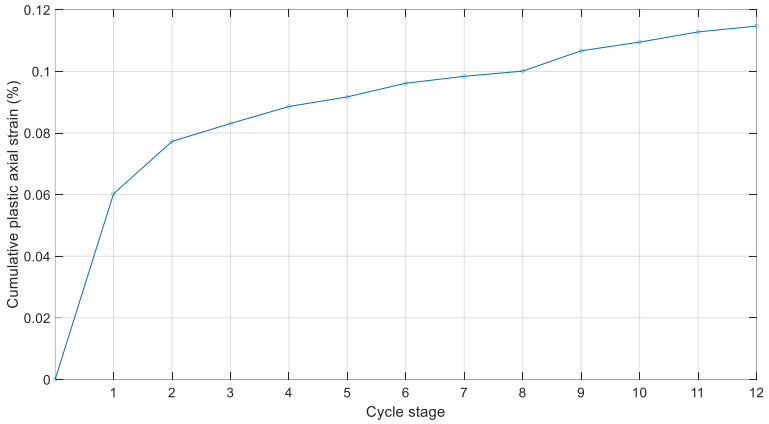

(a) Sample C6 – unreacted

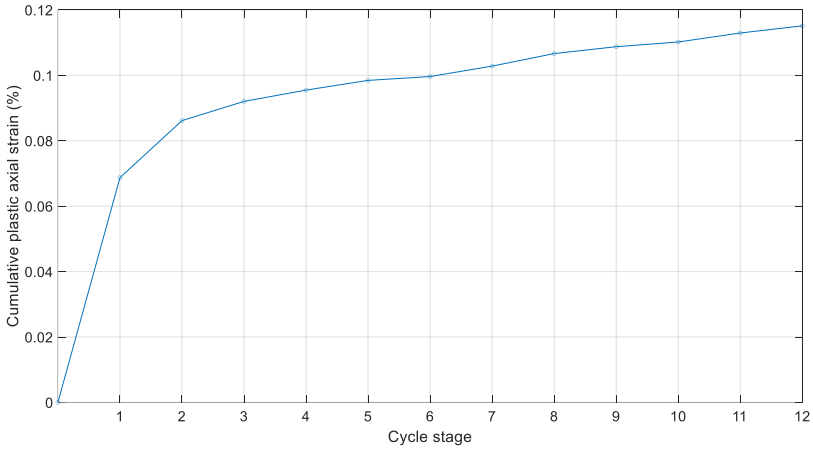

(b) Sample A1 – N_2/2 month

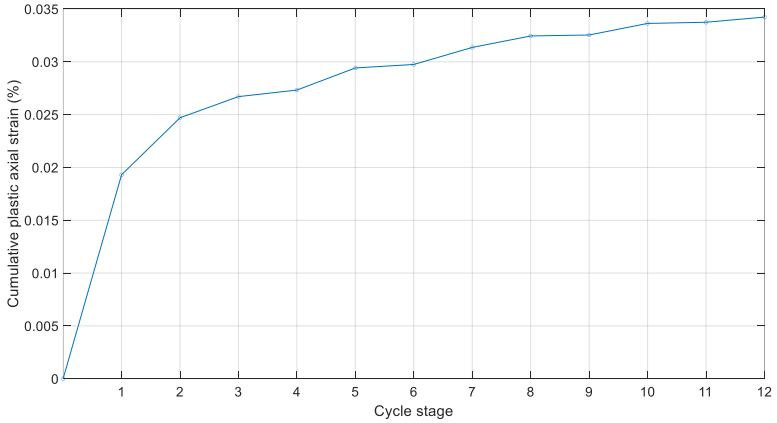

(c) Sample A15 – H_2/2 month

Figure 13. Cumulative plastic strain from the cyclic test of samples (a) C6, (b) A1, and (c) A15 during the stress cycle.

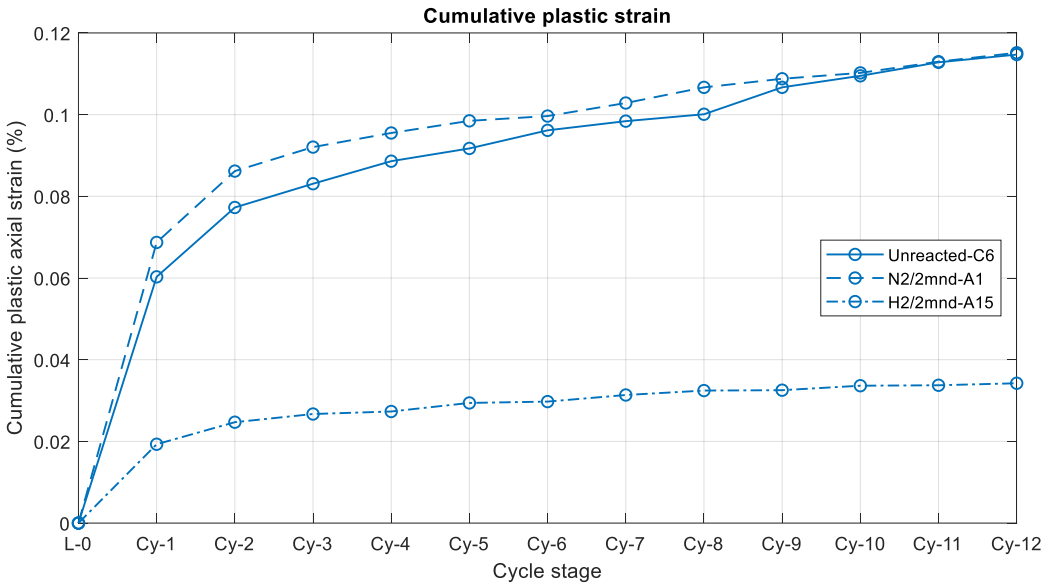

Figure 14. Plastic strain from the cyclic test of all samples C6 (unreacted), A1 (H_2/2 month), and A15 (N_2/2 month) during the stress cycle.

Post-mortem analysis on the cement samples tested without confinement in the UCS test and with 8 MPa confining pressure in the cyclic test shows that brittle failure is more pronounced in the unconfined sample, as shown in Figure 15. It suggest that compaction and pore collapse during failure are more important in confined tests compared to unconfined tests where fracturing (axial splitting) is more important.

Figure 15. Visual observation of samples (left) A15, tested under confinement of 8 MPa and (right) A9, tested without confinement.

4.3 Mineralogical changes during cement exposure

Phases identification of the unexposed cement sample from the XRD analysis shows unreacted phases of alite (C_3S) and brownmillerite (C_4AF). Despite the fast hydration kinetics of alite, the remaining alite can be explained by the formation of a denser layer of the C-S-H phase around the alite surfaces that hinders further hydration due to the high curing temperature (Nelson & Guillot, 2006). Residual alite has also been reported in the phase identification of class G cement cured at 60° C (Ter Heege et al., 2019a, b). The residual C_4AF

is also typically observed in the set cement (Bahafid et al., 2017; Duguid et al., 2017; Ter Heege et al., 2019a, b).

The reacted phase of katoite is indicated in the XRD results. Katoite is a cubic form of calcium aluminate hydrate, which is the product of C_3A hydration when gypsum is absent and a member of the hydrogarnet group. Katoite is a stable form of calcium aluminate hydrate and is directly formed at a high curing temperature (Nelson & Guillot, 2006). When gypsum is added to cement clinker, the hydration of C_3A resulted in ettringite. At an elevated temperature, the stability of ettringite reduces and the development of katoite is more favoured (Bahafid et al., 2017). In this study, the XRF analysis of the cement clinker is not available. However, an existing study (Ter Heege et al., 2019a, b) suggested that gypsum is not present in the Dyckerhoff Class-G cement clinker that is also used in this study. This might explain the absence of ettringite in the XRD analysis. The mineral hibschite is present as a minor phase. It is a member of the hydrogarnet group, similar to katoite, with x=0.2-1.5. This phase has been reported to present as a hydration product of oil well cement (Bahafid et al., 2017). Besides katoite, the portlandite phase from the by-product of C_3S and C_2S hydration is also present.

The XRD analysis shows that there are no significant phase changes in unexposed- and exposed samples. The intensity of the identified peaks of portlandite, alite, hibschite, brownmillerite, and katoite of the samples is relatively similar. Brucite that presents in the H_2-exposed sample is more likely a precipitation product of limewater-saturated brine due to the reaction between $MgCl_2$ and $Ca(OH)_2$. Halite that is observed in both exposed samples is more pronounced at the bottom part of the cores. There are a few unidentified peaks present in the samples that could not be correlated to the cement hydration products, which could be unidentified cement phase or due to contamination (e.g. curing mould substances).

5 Conclusions

In this study, new experimental data is presented of the effects of H_2 exposure and cyclic loading on mechanical properties of oilwell cement, relevant for underground hydrogen storage operations. Changes in mechanical properties (Young's modulus, Poisson's ratio and ultimate strength) have been analyzed using unconfined compressive strength (UCS) tests and confined cyclic loading tests on class G cement samples that were unreacted (cured for 3 days at 80°C) and exposed to lime-saturated brine and N_2 or H_2 for 1 and 2 months. Changes in cement mineralogy were analyzed by XRD analysis of the unreacted and exposed samples.

The main conclusion is that effects of H_2 exposure and cyclic loading on mechanical properties and mineralogical changes of class G cement is limited compared to unreacted or N_2 exposed samples for the investigated conditions. There is no indication that changes in mechanical properties of cement are such that cement integrity of wells used for underground hydrogen storage will be significantly affected. It should be emphasized that this conclusion is based on experiments on one type of cement (class G) and a limited set of conditions. In particular, additional tests to assess the reproducibility of current results and tests on samples that were exposed longer to H_2 and N_2 are of interest. Detailed effects of changing properties for the durability and integrity of wells can be derived by performing a parameter sensitivity analysis with well integrity modelling (cf. WP6) for the range in mechanical properties measured in this study.

The main findings include:

- Exposure of Portland class-G cement to lime-saturated brine and H_2 for 1 and 2 months has limited influence on the mechanical properties. The difference in average values for Young's modulus and ultimate strength from two repeated tests are minor when comparing H_2-exposed samples to unexposed samples or samples exposed to inert N_2. The only difference is that N_2 and H_2 exposure seems to increase the variation in Young's modulus and ultimate strength, but this observation needs to be confirmed in additional tests.
- The mechanical properties of elastic modulus and Poisson's ratio are within the expected range of an oilwell cement. The change in mechanical properties in response to cyclic stress unloading-loading is similar for both exposed and unexposed samples.
- Irreversible (plastic) deformation (compaction) affects measurements of elastic moduli of cement which increases with subsequent load cycles due to the sample compaction. Dynamic Young's modulus and Poisson's ratio derived from acoustic velocity measurements shows limited variation, in particular if static and dynamic Young's modulus are compared. During failure of unconfined samples clear fractures (axial splitting) occurs while failure of confined samples involved more distributed strain and compaction (pore collapse).
- The mineralogical identification using XRD qualitative analysis shows the presence of residual alite, residual brownmillerite, portlandite, katoite, and hibschite in both unexposed and exposed (H_2 and N_2) samples. The change in intensity of these phases between unexposed and H_2- and N_2-exposed samples is minor, although XRD patterns indicate some minerals that could not be identified.

6 References

Bahafid, S., Ghabezloo, S., Duc, M., Faure, P., & Sulem, J. (2017). Effect of the hydration temperature on the microstructure of Class G cement: C-S-H composition and density. Cement and Concrete Research, 95, 270-281.

Boersheim, E. C., Reitenbach, V., Albrecht, D., Pudlo, D., & Ganzer, L. (2019, 2019). Experimental Investigation of Integrity Issues of UGS Containing Hydrogen. Paper presented at the SPE Europec featured at 81st EAGE Conference and Exhibition, London, UK.

Corina, A. N., & ter Heege, J. (2021). WP-D Wells of the KIP2021 Subsurface Energy Storage.

Corina, A.N., Zikovic, V., Soustelle, V. & Ter Heege, J.H. (2022). Review of current practices and existing experimental data for well and rock materials under cyclic hydrogen injection and withdrawal. H2020 HyUSPRe project report D5.1, 60 pp.

Duguid, A., Butsch, R., Carey, J. W., Celia, M., Chugunov, N., Gasda, S., et al. (2017). Baseline integrity property measurement of legacy oil and gas wells for carbon storage projects. Greenhouse Gases: Science and Technology, 7(5), 866-890.

Jacquemet, N., Chiquet, P., & Grauls, A. (2020). Hydrogen Reactivity with (1) a Well Cement - PHREEQC Geochemical Thermodynamics Calculations. 2020(1), 1-5.

Kuanhai, D., Yue, Y., Yi, H., Zhonghui, L., & Yuanhua, L. (2020). Experimental study on the integrity of casing-cement sheath in shale gas wells under pressure and temperature cycle loading. Journal of Petroleum Science and Engineering, 195, 107548.

Nelson, E. B., & Guillot, D. (2006). Well cementing (2nd ed. ed.). Texas, USA: Schlumberger.

Reddy, B. R., Santra, A., McMechan, D., Gray, D., Brenneis, C., & Dunn, R. (2007). Cement Mechanical-Property Measurements Under Wellbore Conditions. SPE Drilling & Completion, 22(01), 33-38.

Shi, Z., Jessen, K., & Tsotsis, T. T. (2020). Impacts of the subsurface storage of natural gas and hydrogen mixtures. International Journal of Hydrogen Energy, 45(15), 8757-8773.

Smith, D.K. 2003. Cementing. Monograph Series, SPE, Richardson, Texas 4, Chaps. 2 and 3.

Szabó-Krausz, Z., Gál, N.E., Gável, V., Falus, G. (2020). Wellbore cement alteration during decades of abandonment and following CO_2 attack – A geochemical modelling study in the area of potential CO_2 reservoirs in the Pannonian Basin. Applied Geochemistry 113, 104516.

Ter Heege, J.H., Vercauteren, F., Pipilikaki, P., Wollenweber, J., & Naumann, M. (2019a). Deliverable D3.2 Report on adaptation of cement formulations.: GeoWell: Innovative materials and designs for long-life high-temperature geothermal wells.

Ter Heege, J.H., Wollenweber, J., Naumann, M., Pipilikaki, P., Vercauteren, F. (2019b). Well integrity of high temperature wells: Effect of mineralogical changes on mechanical properties of well cement. 53rd US Rock Mechanics/Geomechanics Symposium held in New York, NY, USA, 23–26 June 2019. ARMA 19–1981 (www.onepetro.org).

Underground Sun Storage. (2020). Final Report Public 13.

Watson, T.L. and Bachu, S. (2009). Evaluation of the Potential for Gas and CO2 Leakage Along Wellbores. *SPE Drilling & Completion* 24, 115-126.

Yousuf, N., Olayiwola, O., Guo, B., Liu, N. (2021). A comprehensive review on the loss of wellbore integrity due to cement failure and available remedial methods. Journal of Petroleum Science and Engineering, 207, 109123.

Zhang, J. F., Liu, K., Hou, R. X., Wang, B., & Yang, J. L. (2014). Development and change of compressive strength for class G oil well cement under high temperature. Advanced Materials Research, 941. 1441-1444.

Zhou, S., Liu, R., Zeng, H., Zeng, Y., Zhang, L., Zhang, J., et al. (2019). Mechanical characteristics of well cement under cyclic loading and its influence on the integrity of shale gas wellbores. Fuel, 250, 132-143.

Appendix A Stress strain curves

Sample B2 (unreacted / UCS test)

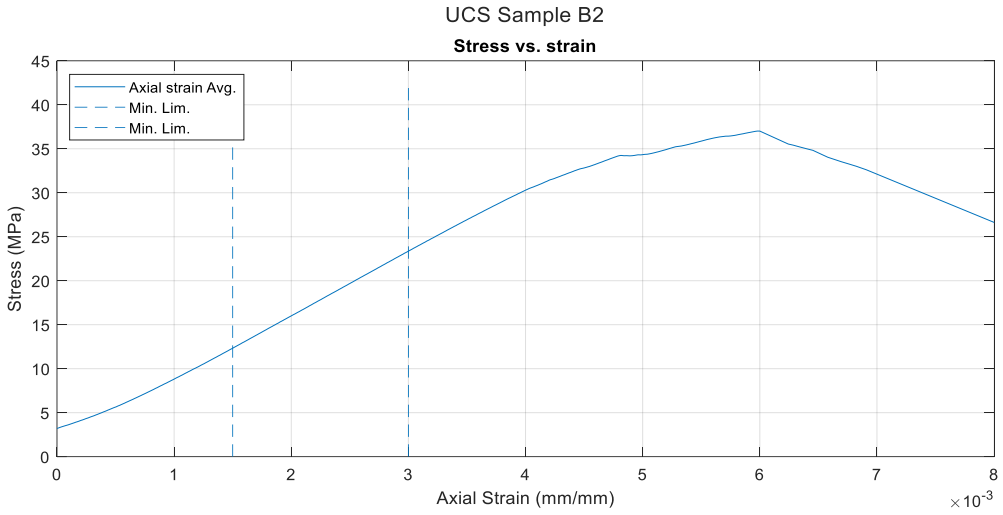

Figure 16. Stress-strain curve of sample B2.

Sample C2 (unreacted / UCS test)

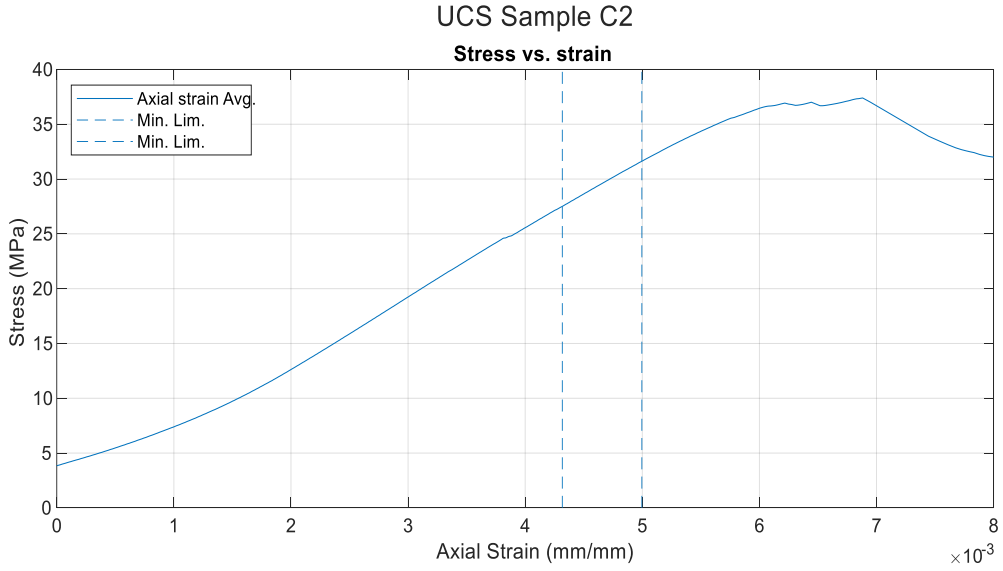

Figure 17. Stress-strain curve of sample C2.

Sample C6 (unreacted / cyclic test)

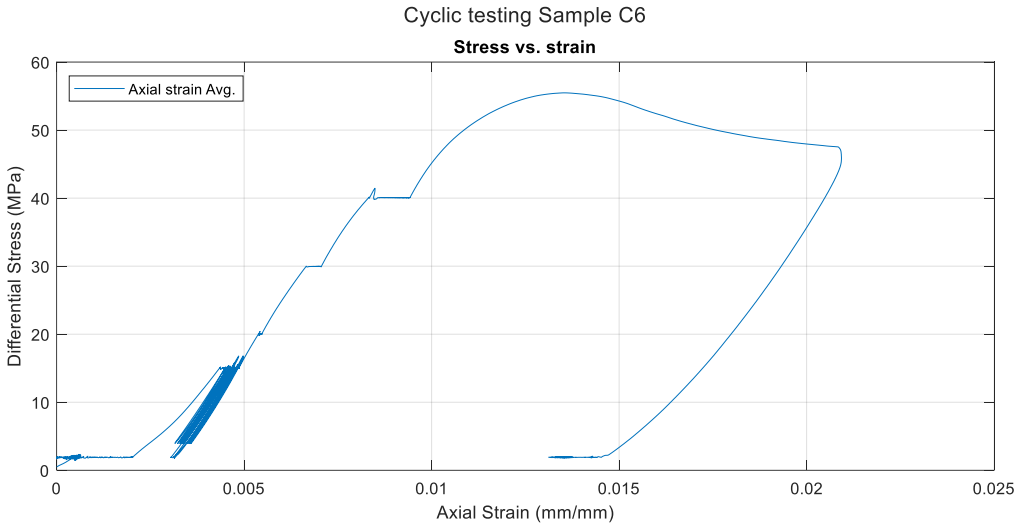

Figure 18. Stress-strain curve of sample C6.

Sample B8 (N_2-1 month / UCS test)

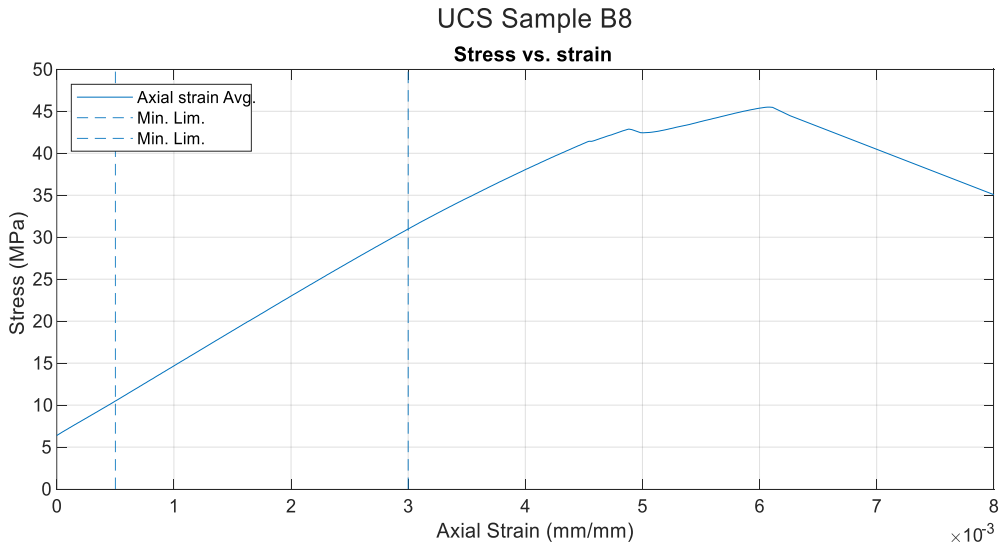

Figure 19. Stress-strain curve of sample B8.

Sample B5 (N_2-1 month / UCS test)

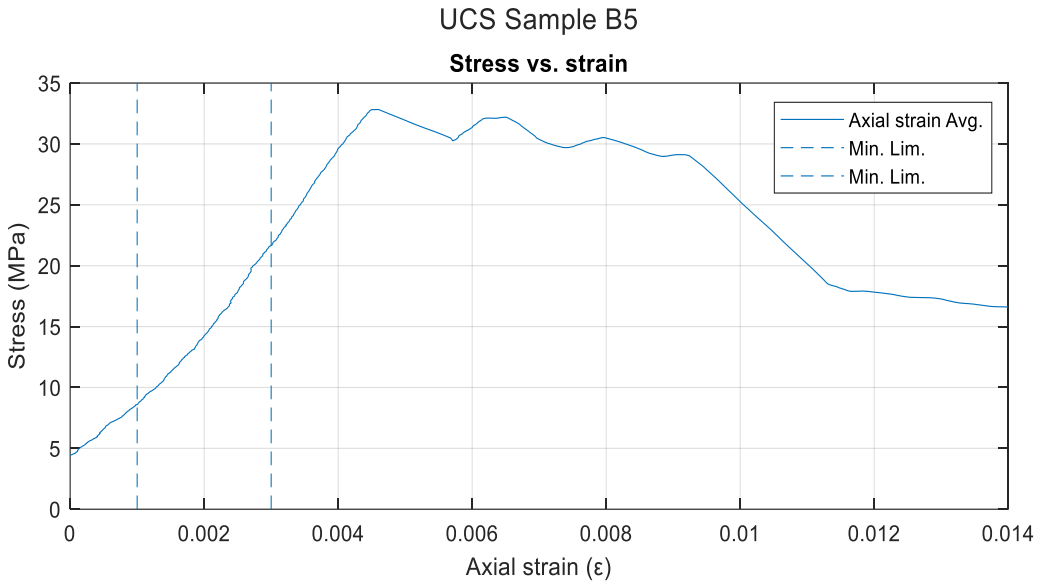

Figure 20. Stress-strain curve of sample B5.

Sample A17 (N_2-2 month / UCS test)

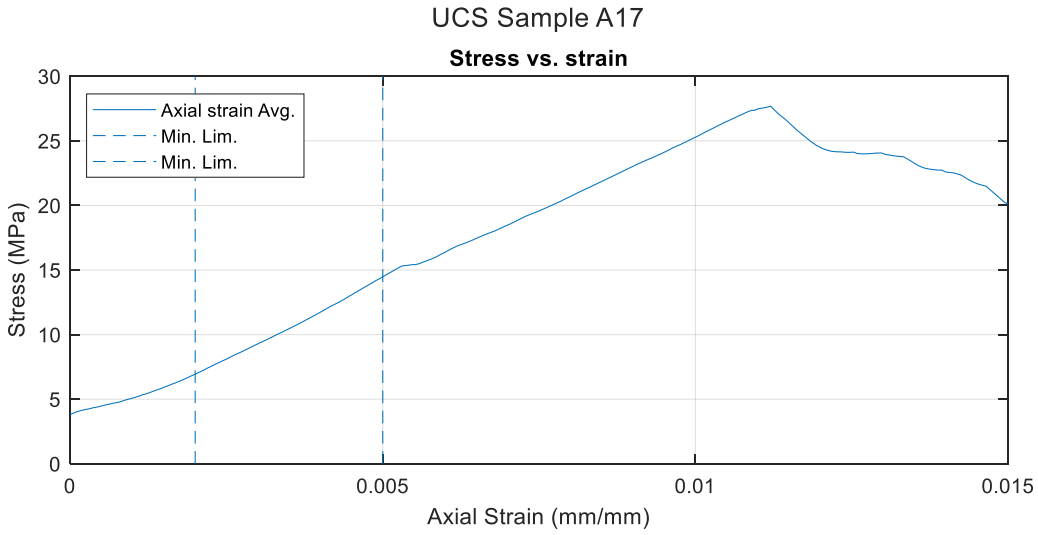

Figure 21. Stress-strain curve of sample A17.

Sample C9 (N_2-2 month / UCS test)

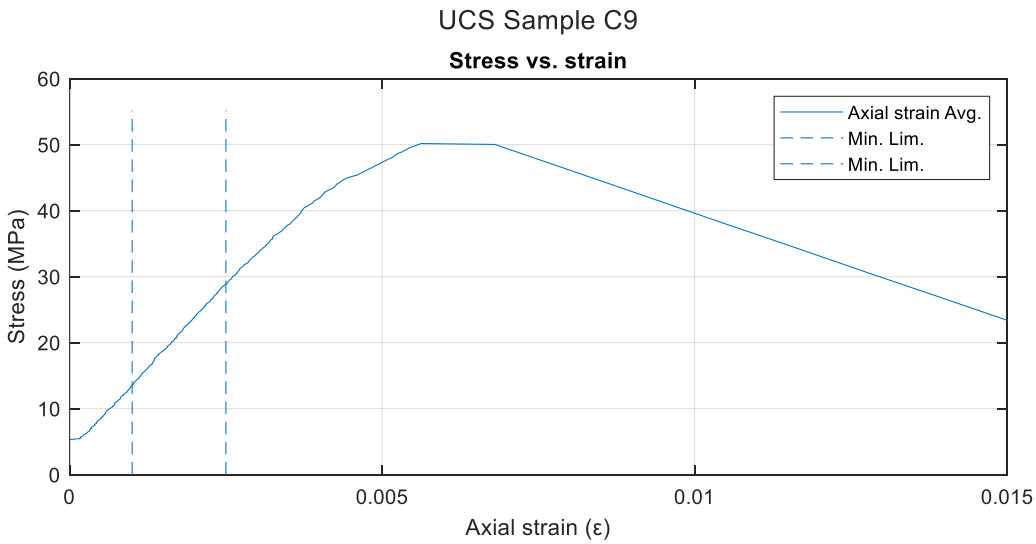

Figure 22. Stress-strain curve of sample C9.

Sample A1 (N_2-2 month / Cyclic test)

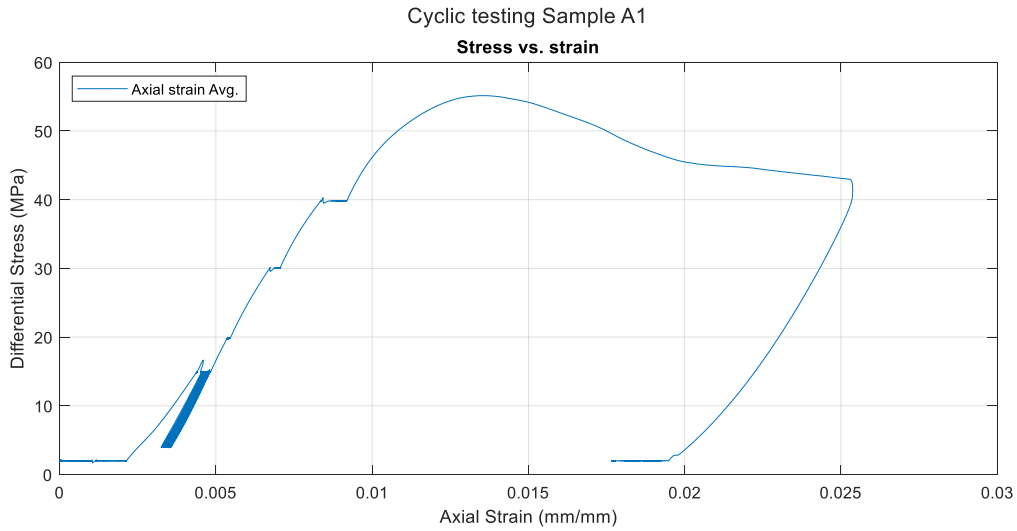

Figure 23. Stress-strain curve of sample A1.

Sample C18 (H_2-1 month / UCS test)

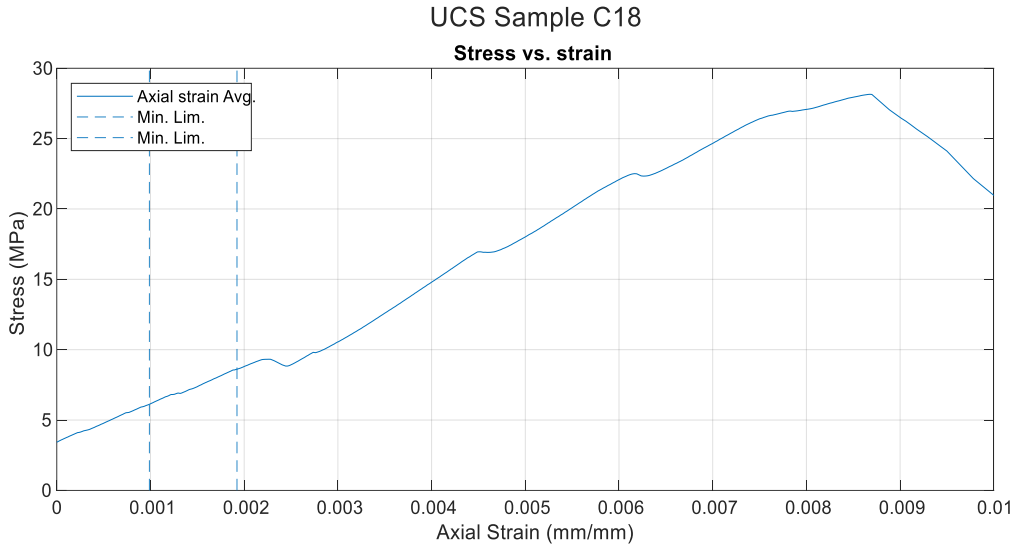

Figure 24. Stress-strain curve of sample C18.

Sample A9 (H_2-1 month / UCS test)

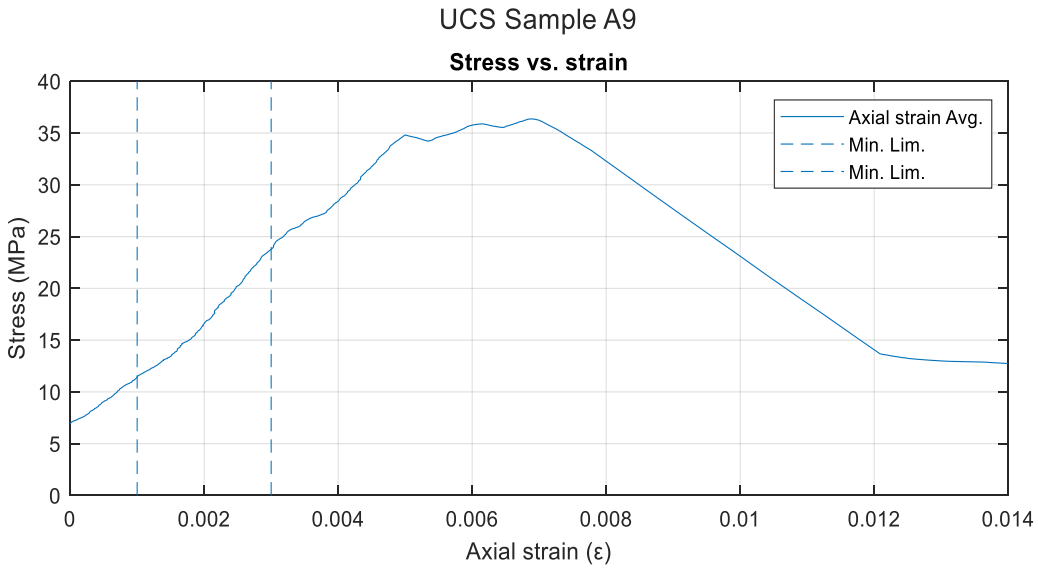

Figure 25. Stress-strain curve of sample A9.

Sample C10 (H_2-2 month / UCS test)

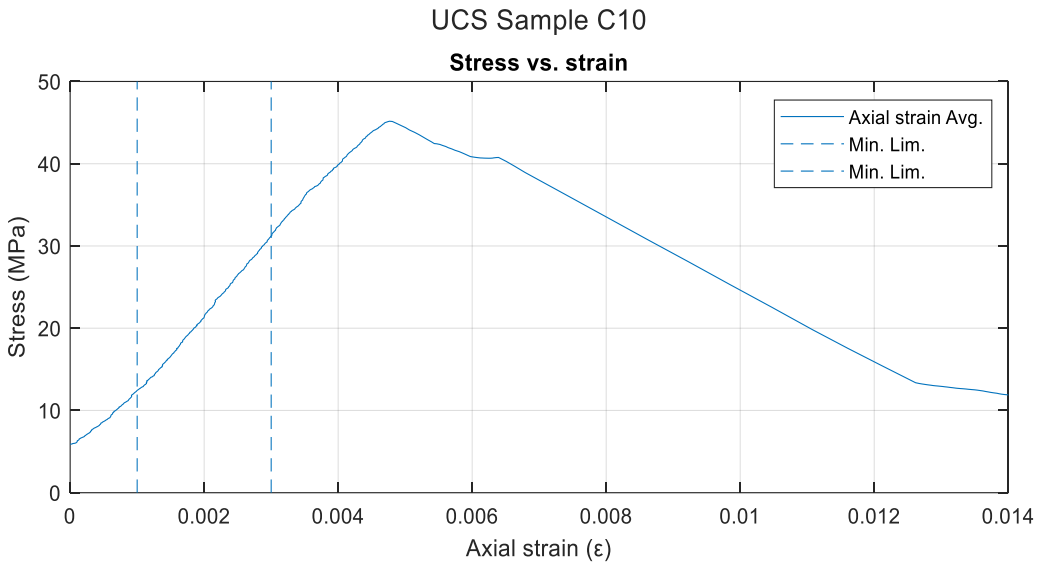

Figure 26. Stress-strain curve of sample C10.

Sample A4 (H_2-2 month / UCS test)

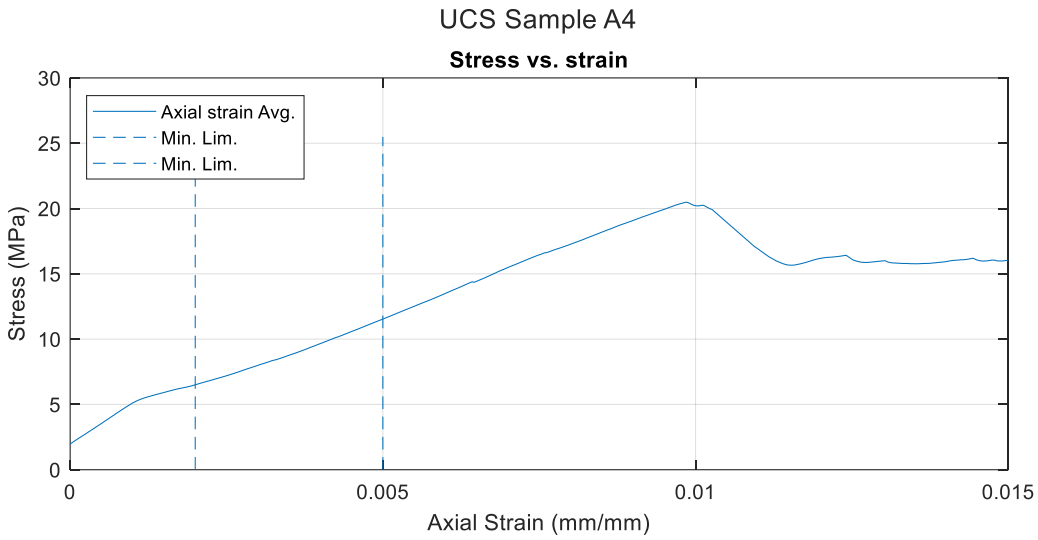

Figure 27. Stress-strain curve of sample A4.

Sample A15 (H_2-2 month / UCS test)

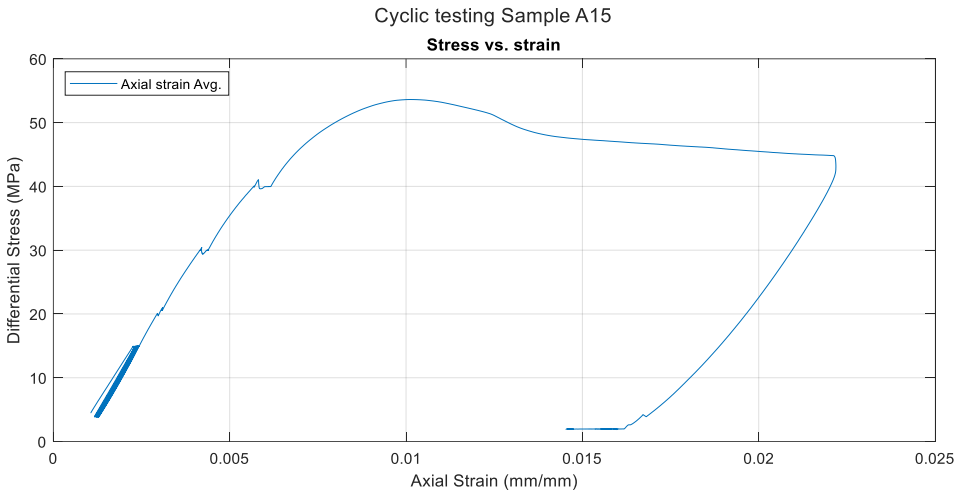

Figure 28. Stress-strain curve of sample A15.

Stress-strain curves UCS tests

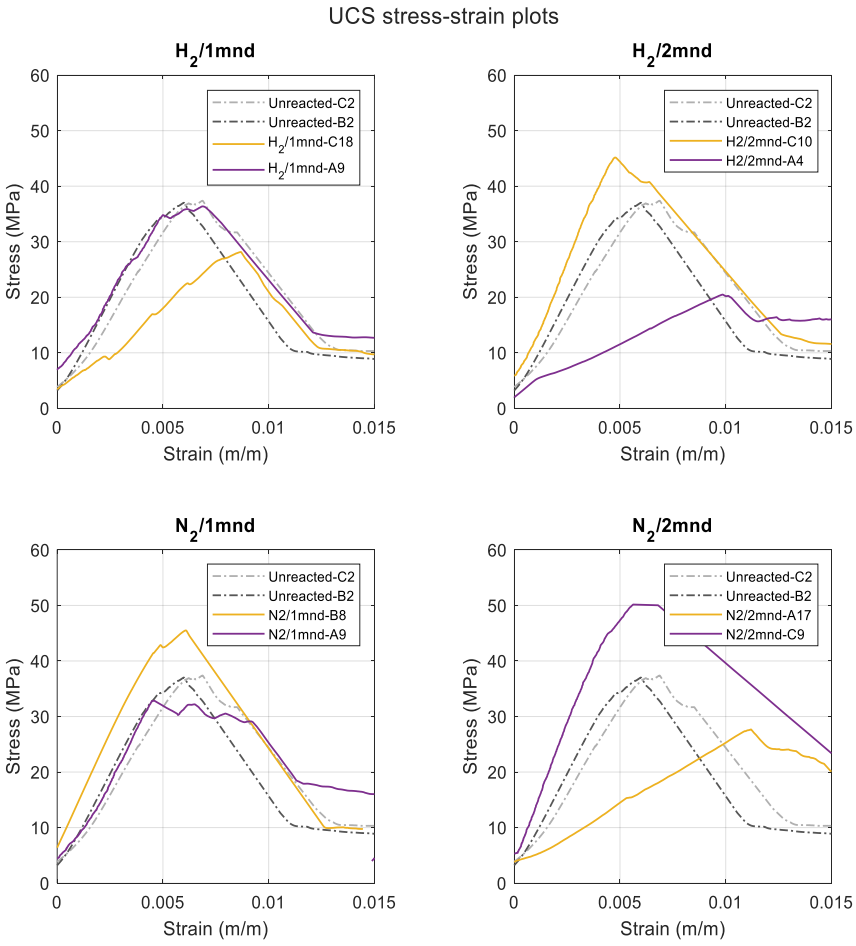

Figure 29. Stress-strain curves of all samples from UCS tests grouped by the exposure period and condition.